Antileishmanial activity of new hybrid tetrahydroquinoline and quinoline derivatives with phosphorus substituents.

Ana Tejería,[§] Yolanda Pérez-Pertejo,[§] Rosa M. Reguera,[§] Rubén Carbajo-Andrés,[§] Rafael Balaña-Fouce,[§,*] Concepción Alonso,[#] Endika Martin-Encinas,[#] Asier Selas,[#] Gloria Rubiales,[#] and Francisco Palacios[#,*]

[§]*Departamento de Ciencias Biomédicas; Universidad de León, Campus de Vegazana s/n; 24071 León (SPAIN), Phone 34 987 291590.*

[#]*Departamento de Química Orgánica I, Facultad de Farmacia and Centro de Investigación Lascaray (Lascaray Research Center). Universidad del País Vasco/Euskal Herriko Unibertsitatea (UPV/EHU). Paseo de la Universidad 7, 01006 Vitoria-Gasteiz, Spain.*

Keywords: Leishmania, phosphorus substituted quinoline derivatives, DNA-topoisomerase

Abbreviations: VL, Visceral Leishmaniasis; TopIB, Type IB DNA Topoisomerase; IRFP, Infra Red Fluorescent Protein; FCS, Fetal Calf Serum; DMSO, Dimethyl sulfoxide; SI, Selectivity Index; CPT, camptothecin; CPTs, camptothecin derivatives; QUIN, quinoline; THQ, tetrahydroquinoline; HDAr, hetero-Diels-Alder reaction; TLC, thin layer chromatography; MEPS, Molecular Electrostatic Potential Surface; DFT: Density Functional Theory; HOMO-LUMO, Highest Occupied Molecular Orbitals – Lowest Unoccupied Molecular Orbitals; n-ROTB, number of Rotatable Bonds.

ABSTRACT. Visceral leishmaniasis is a neglected parasitic disease that affects humans in low-income countries with no effective prophylactic vaccine available at present. With the exception of miltefosine, antimony derivatives and amphotericin B – the first-line drugs in use – need parenteral administration, are unsafe and can be the origin of resistant strains. For these reasons, there are numerous initiatives dedicated to the search for new antileishmanial compounds that are more effective and that are designed to inhibit recognized targets in the parasite. Eukaryotic type I DNA topoisomerase is an essential enzyme for the viability of *Leishmania*, and due to its structural differences with the human enzyme, represents a promising druggable target for the development of new compounds against this disease. In this search, heterocyclic compounds, such as hybrid tetrahydroquinoline and quinoline derivatives with phosphorated groups, have been prepared by multicomponent cycloaddition reaction between phosphorus-substituted anilines, aldehydes and styrenes. The antileishmanial activity of these compounds has been evaluated on both promastigotes and intramacrophagic amastigotes of *Leishmania infantum*. In addition, the cytotoxic effects of newly synthesized compounds were assessed on host murine splenocytes in order to calculate the corresponding selective indexes. Good antileishmanial activity of functionalized tetrahydroquinolines **4a**, **5a, 6b** and quinoline **8b** has been observed with similar activity than the standard drug amphotericin B and close selective index (SI between 43 and 57) towards *L. infantum* amastigotes to amphotericin B. Special interest shows tetrahydroquinolylphosphine sulfide **5a** with an EC_{50} value (0.61 ± 0.18 μM) similar to the standard drug amphotericin B (0.32 ± 0.05 μM) and selective index (SI = 56.87). In addition, compound **4c** shows remarkable inhibition on *Leishmania* topoisomerase IB. However, despite these interesting results, further studies are needed to disclose other potential targets involved in the antileishmanial effect of these novel compounds.

1. Introduction

Visceral leishmaniasis (VL) is a parasitic-borne disease that affects more than 300.000 people in four of the five Continents and causes 30.000 deaths every year most of them in East Africa [1,2]. For decades, the standard treatment against human VL was based on the administration of systemic drugs derived from pentavalent antimony (Sb^V) [3]. However, the use of these drugs is associated with nephrotoxic and cardiotoxic side effects [4] and what is even worse, their continued administration as first-choice medicines along with the contamination of drinking water with arsenic salts has driven to a further increase of resistant strains, especially in the north of Indian subcontinent [5,6]. The emergence of all these issues has produced an alarming increase in treatment failures and relapses [7]. Among the second-line drugs amphotericin B (AmB), deoxycholate or liposomal, is the most currently used [8]. Liposomal AmB (AmBisome, Gilead) is an effective antileishmanial medicine but has some drawbacks; it requires slow intravenous administration, is costly and chemically unstable under extreme field conditions [9]. Finally, miltefosine (Figure 1), the first oral drug approved against VL, has been related to teratogenic issues and cannot be administered to pregnant women and newborns [10,11]. Combinations of all these compounds – to which the antibiotic paromomycin must be included – has been recommended by Drugs for Neglected Diseases initiative (DNDi) with good results in endemic countries of Asia and Africa [12].

Although many efforts have been done to identify new druggable targets against VL, the overall output of new antileishmanial compounds is poor, owing in part to the specific interactions of the parasite with the host. Therefore, the demand for new drugs and new targets is nowadays an urgent need more than ever. Eukaryotic DNA topoisomerase I (TopIB) is a nuclear enzyme involved in controlling DNA topology in

many essential metabolic processes of eukaryotic cells. To perform these functions, TopIB introduces single cuts in DNA skeleton by nucleophilic attack of the catalytic tyrosine on the phosphodiester bonds of DNA double helix, forming transient single-strain covalent cleavage complexes with DNA [13,14]. These transient intermediates are rapidly reversed in physiological circumstances through the 5'-OH attack of the nicked chain in the TopIB-DNA phosphotyrosyl complex, thus restoring the intact DNA and releasing the free enzyme [15,16]. This circumstance has been used to specifically target TopIB with small molecules that ultimately can prevent cell growth. In this regard, many TopIB inhibitors called poisons, such as the plant alkaloid camptothecin (CPT, Figure 1), establishes hydrogen bonds between TopIB and DNA resulting in the stabilization of covalent cleavage complex, resulting in an increased genomic fragility during replication, transcription or recombination processes [17]. Other compounds are mere catalytic inhibitors of TopIB preventing the binding of TopIB with DNA [18]. The value of TopIB as target in proliferative processes was validated with four CPT analogues that have been approved by different agencies for the clinical treatment of cancers, including irinotecan and topotecan (in USA and Europe), belotecan (in South Korea) and 10-hydroxycamptothecin (in China) [19-21].

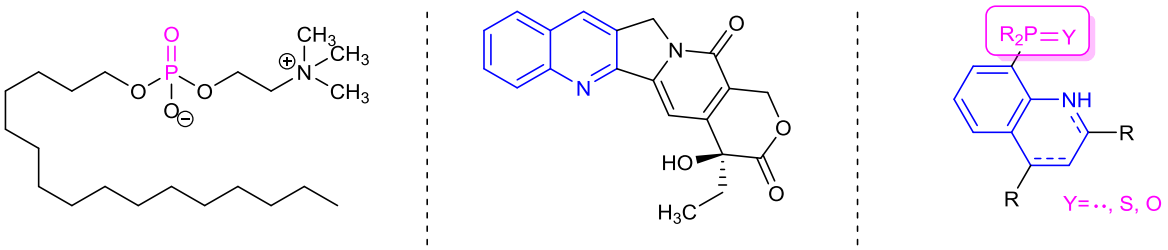

Figure 1. Structure of miltefosine (left), camptothecin (middle) and newly phosphorated tetrahydroquinolines and quinolines (right).

Previous studies of our group have shown that TopIB from trypanosomatids – including *Leishmania* (LTopIB) – is structurally different from the human enzyme (hTopIB) and it is selectively induced during the growth of the parasites inside the host [22,23]. In this regard, several families of compounds either poisons and inhibitors, have been successfully screened against LTopIB, thus pointing this enzyme as an interesting druggable target against leishmaniasis [24-26].

The development of hydrid molecules is an innovative approach for the discovery of new drugs [27], since the presence of two pharmacophores in a single molecule may synergize their biological effects [28]. The new compounds synthesized in this report are based on the molecular hybridization [29] of the flat or quasi-planar heterocyclic structure of tetrahydroquinoline (THQ) [30] or quinoline (QUIN) [31] present in a wide number of natural products and active pharmaceutical ingredients with therapeutic effects with various phosphorus substituents such as phosphine, phosphine sulfide and phosphine oxide (Figure 1, right). Organophosphorus derivatives are interesting compounds since phosphorus substituents may affect the reactivity of heterocycles and regulate important biological functions [32]. The development of new strategies for the preparation of aminophosphonates [33], phosphinated [34], or phosphorylated azaheterocycles [35] implies the incorporation of organophosphorus functionalities in simple synthons. For example, the diphosphonylation of quinolines leads to tetrahydroquinolines [36] and phosphorated derivatives of quinolines (ciprofloxacin, norfloxacin, sparfloxacin) are characterized by a greater biological activity than the original drugs [37]. Thus, from cyclophosphamide [38] used to treat leukemia and different cancers to brigatinib [39], which contains a phosphine oxide group approved in the USA for the treatment of metastatic non-small cell lung cancer (NSCLC) [40], a

large number of compounds containing phosphorus such as antibiotics phosphinothricin, fosfomycin, fosfidomycin or dehydrophos [41] have been described.

A wide range of six-membered nitrogen-containing heterocyclic compounds play a major role in organic chemistry through their widespread presence in nature and in their consequent biological activity with applications in biochemistry, pharmacology and material science [42,43]. Many strategies are described in the literature for the synthesis of nitrogenated heterocycles, among which one of the most straightforward is the hetero-Diels-Alder reaction (HDAr). This reaction type is an atom-economic alternative for the carbon-carbon and carbon-heteroatom bond construction [44] and represents an excellent tool for the generation of six-membered rings with a high molecular complexity [45], which may have industrial applications [46]. Among those strategies, the Povarov reaction [47,48] allows the preparation of nitrogen-containing heterocyclic compounds in an excellent way [49,50]. This methodology also represents a direct route to the tetrahydroquinoline (THQ) and quinoline (QUIN) core structure of interesting biologically active compounds [51] as TopIB inhibitors and with antiproliferative activity against several cancer cell lines as reported in our research group [52], so we thought that it could work against experimental infections of *Leishmania* parasites. It is well known that a wide range of lead compounds with fused nitrogen-containing heterocycles – camptothecins, indenoisoquinolines, naphthyridines, and others – are inhibitors of TopIB and display strong antileishmanial activity [53].

This manuscript describes the synthesis of hybrid THQ and QUIN containing phosphorus substituents such as phosphine, phosphine sulfide and phosphine oxide groups by multicomponent cycloaddition reaction between phosphorus substituted anilines, aldehydes and styrenes as well as the antileishmanial effect of a new series of hybrid substituted QUIN compounds on *L. infantum*, the eukaryotic pathogen

responsible for VL at both shores of the Mediterranean basin. In this regard, we carried out a full screening of these compounds on the two forms of the parasite, free-living promastigotes and amastigotes infecting primary mouse splenocytes, which were isolated from BALB/c mice that had been previously inoculated with *L. infantum*-iRFP, a transfected strain that emits fluorescence in the near infrared spectrum. In addition, the inhibitory effect of these compounds, both *in silico* and on recombinant hTopIB and LTopIB enzymes *in vitro*, was evaluated in order to identify their potential mechanism of action. Finally, a predictive study was also carried out to select those compounds with better therapeutic profile for further *in vivo* studies.

2. Chemistry

We started with the synthesis of functionalized THQ and QUIN containing phosphorated groups by multicomponent Povarov type [4+2]-cycloaddition reaction. In this sense, the *endo*-1,2,3,4-tetrahydroquinolinylphosphines **4** were regioselectively obtained by reaction between aldehydes **1a** (R = C_6H_5), **1b** (R = 4-FC_6H_4) or **1c** (R = 4-$MeOC_6H_4$), 2-(diphenylphosphino)aniline **2a** and *p*-fluorostyrene **3a** (R^1 = F) or *p*-methylstyrene **3b** (R^1 = CH_3) in the presence of 2 equivalents of $BF_3{\cdot}Et_2O$ in refluxing chloroform (Scheme 1, Chart 1).

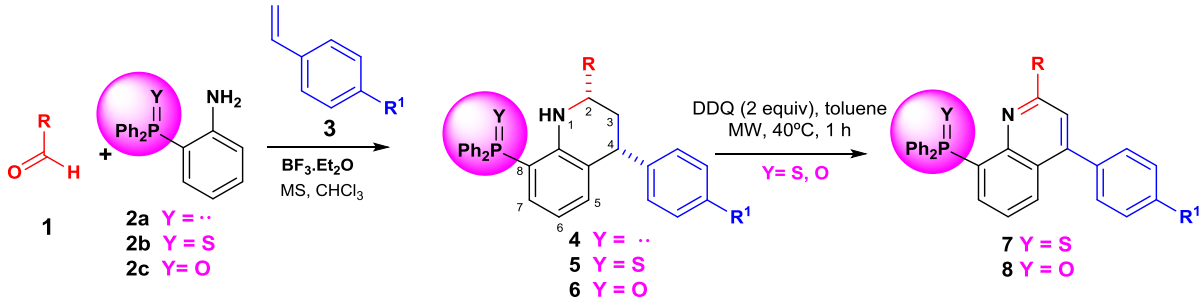

Scheme 1. Syntheses of 1,2,3,4-tetrahydroquinolinyl-phosphines **4**, -phosphine sulfides **5**, -phosphine oxides **6**, quinolinyl-phosphine sulfides **7** and -phosphine oxides **8**.

The formation of 1,2,3,4-tetrahydroquinolinylphosphines **4** may be explained through a regio- and stereoselective [4+2]-cycloaddition reaction between aldimine, obtained from aldehyde **1** and amine **2a**, and the corresponding olefin **3**, followed by a prototropic tautomerization as previously reported [54].

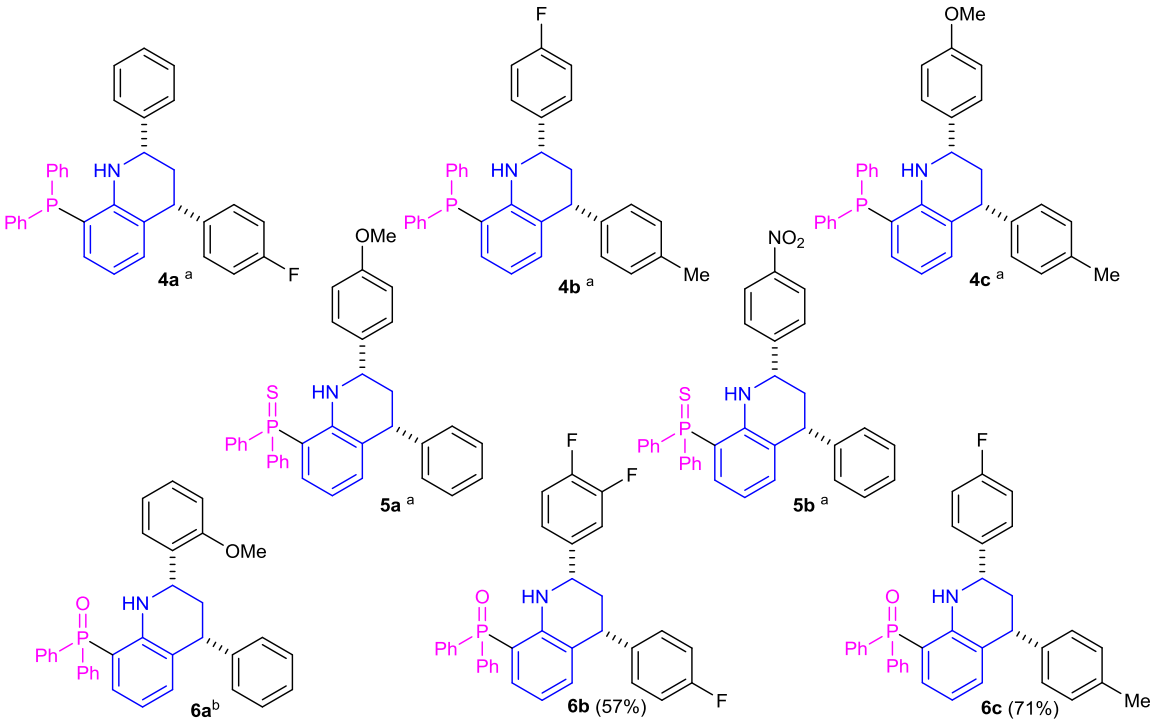

Chart 1. Structures of 1,2,3,4-tetrahydroquinolinylphosphines **4**, -phosphine sulfides **5**, and -phosphine oxides **6** obtained by multicomponent Povarov reaction. [a]Reference [54]. [b]Reference [52].

Along with phosphine the tetrahydroquinoline-phosphine sulfides as well as -phosphine oxides constitute an important class of organophosphorus compounds with potential biological activity [32]. For this reason, next we explored the preparation of THQ and QUIN derivatives with the other phosphorus substituents. The three components, aldehydes **1**, 2-(diphenylphosphine sulfide)aniline **2b** (Y = S) or 2-(diphenylphosphine oxide)aniline **2c** (Y = O) and olefins **3** (Scheme 1) were mixed in the presence of the Lewis acid ($BF_3 \cdot Et_2O$), and corresponding *endo*-1,2,3,4-tetrahydroquinolinylphosphine sulfides **5** (Y = S) or *endo*-1,2,3,4-tetrahydroquinolinylphosphine oxides **6** (Y = O) were respectively obtained in refluxing chloroform after 24-48 hours (Chart 1) in a

regioselective way. As before, the formation of 8-phosphine sulfide- **5** or 8-phosphine oxide-1,2,3,4-tetrahydroquinolines **6** may be explained through a regio- and stereoselective [4+2]-cycloaddition reaction between aldimines, initially generated by condensation reaction of aldehydes **1** and functionalized anilines **2**, and olefins **3** followed by a prototropic tautomerization.

Subsequent dehydrogenation of THQ **5** (Y = S) and **6** (Y = O) with 2 equivalents of DDQ in toluene under microwave irradiation produced the corresponding quinolinyl-phosphine sulfides **7** (Y = S) and -phosphine oxides **8** (Y = O; Scheme 1, Chart 2). The formation of compounds **7** and **8** was determined by ^{1}H NMR spectroscopy where upfield signals corresponding to the protons of tetrahydroquinoline ring of starting compounds **5** and **6** disappeared and only aromatic signals were observed. On the other hand, quinolines **8a** and **8b** may be also obtained directly by means of the multicomponent reaction of aldehyde **1**, aniline **2c** and styrenes **3** (see Experimental Section).

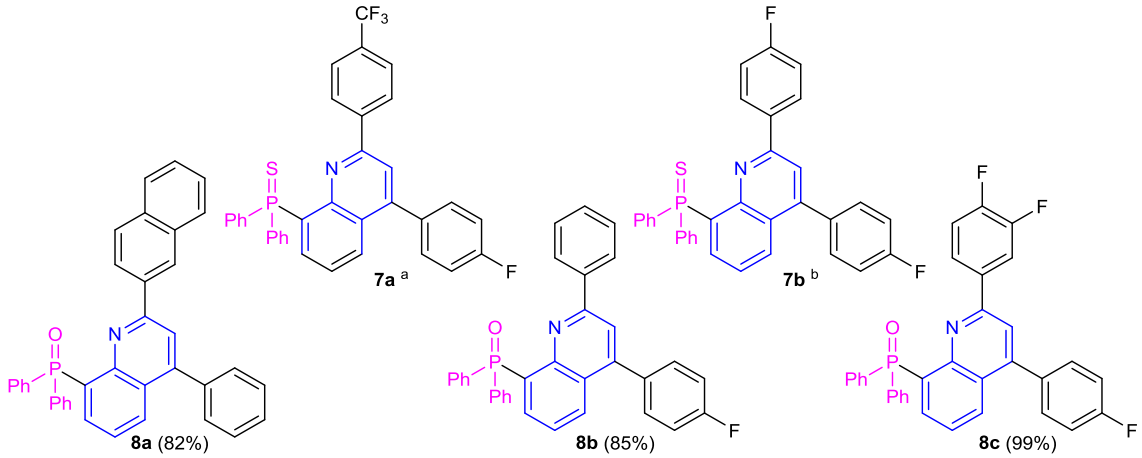

Chart 2. Structures of quinolinyl-phosphine sulfides **7** and -phosphine oxides **8** obtained by dehydrogenation. [a] Reference [54]. [b] Reference [52].

The methodology represents an easy and efficient strategy for the preparation of functionalized THQ **4-6** and QUIN **7**,**8** derivatives containing phosphorus substituents and tolerates a wide range of electron-releasing and electron-withdrawing aromatic

aldehydes, even fluorinated ones which allow the preparation of fluoro containing compounds [55] interesting substrates from a biological point of view. And regarding phosphorus substitution, a diversity of phosphorus derivatives can be prepared, such as phosphine, phosphine oxide and phosphine sulfide derivatives. The biological behavior of prepared new hybrid molecules as TopIB inhibitors and as antileishmanial agents was studied.

3. Biological results and discussion

Antileishmanial activity of a new series of phosphorus substituted THQ and QUIN derivatives. To assess the effect of the newly phosphorus substituted THQ and QUIN derivatives on *L. infantum* parasites, we performed both *in vitro* and *ex vivo* assays on free-living promastigotes and intramacrophage amastigotes, respectively. In this regard, the transgenic *L. infantum* strain *L. infantum*-iRFP, which constitutively express the heterologous *irfp* encoding gene that produces the infrared fluorescent protein iRFP from *Rhodopseudomonas palustris* bacteriophytochrome, allows a rapid and reproducible readout (λexc. 600 nm, λem. 708 nm) of the viable parasites. To resemble closer the physiological environment where the infection takes place, the infected macrophages harboring amastigotes were isolated from BALB/c mice, which had been inoculated with 10^8 *L. infantum*-iRFP metacyclic promastigotes 5 to 6 weeks earlier. After this period, spleens were dissected and the primary culture of splenocytes, which contains naturally infected macrophages, was exposed to the testing compounds [56]. This method has shown series of advantages over classical axenic amastigotes or *in vitro* infections on a standard strain of macrophages: i) it mimics closer the conditions of natural *in vivo* infections; ii) the *ex vivo* conditions where the drug is placed, include the immunological microenvironment that can help to destroy the invading cells within spleen macrophages [57]. Finally, in order to assess the tolerability of testing drugs, a

cytotoxicity assay was performed in free-parasite macrophages obtained under the same conditions but from uninfected BALB/c mice.

The antileishmanial effect of the new series of compounds with the new phosphorus substituted THQ and QUIN derivatives was obtained from dose-response curves by plotting the infrared fluorescence emitted by the viable parasites *vs* different concentrations of the testing compounds (Table 1). Plots were fitted by nonlinear analysis using the Sigma-Plot 10.0 statistical package. For both *L. infantum*-iRFP promastigotes and amastigotes, the drug effect was expressed as the 50%-reduction of infrared emission (EC_{50}) with respect to negative control (that contains the same percentage of DMSO, used as drug solvent).

Table 1. Bioactivity of phosphorylated compounds on both forms of *Leishmania* parasites.

		EC_{50} (μM) *L. infantum*		CC_{50} (μM)	
entry	type	promastigotes	amastigotes	splenocytes	SI
1	**4a**	3.14 ± 0.04	1.75 ± 0.51	90.62 ± 8.11	51.78
2	**4b**	20.91 ± 7.00	1.79 ± 1.33	46.97 ± 5.25	26.24
3	**4c**	27.72 ± 2.36	5.96 ± 0.91	> 50	> 8.4
4	**5a**	10.66 ± 0.53	0.61 ± 0.18	34.69 ± 1.54	56.87
5	**5b**	36.38 ± 1.89	2.73 ± 0.57	57.03 ± 2.39	20.89
6	**6a**	9.39 ± 2.55	0.98 ± 0.73	34.23 ± 1.78	34.93
7	**6b**	6.15 ± 1.24	1.46 ± 0.16	63.70 ± 1.88	43.63
8	**6c**	7.10 ± 0.81	1.85 ± 1.09	13.82 ± 0.39	7.47
9	**7a**	8.83 ± 1.20	>10	89.71 ± 3.21	n.d.
10	**7b**	11.02 ± 3.49	>10	92.06 ± 0.98	n.d.
11	**8a**	4.91 ± 0.38	4.14 ± 1.64	57.11 ± 4.60	13.79
12	**8b**	6.01 ± 0.80	1.39 ± 1.08	71.03 ± 2.11	51.10
13	**8c**	2.33 ± 0.25	2.15 ± 1.23	23.95 ± 1.36	11.14
14	**AMB**	0.77 ± 90.15	0.32 ± 0.05	>20	62.5

Antileishmanial effects (EC_{50} ± SD) on promastigotes and amastigotes of *L. infantum*. Cytotoxicity effects (CC_{50} ± SD) on murine splenocytes. *SI: Selective Index.

For antimicrobial drugs, more important than the killing effect in absolute terms, is the selectivity index (SI) that is a relative measure of the effect of the compound on the target microbe with respect the toxicity in host cells. The SI of each compound was calculated from the ratio between their cytotoxicity on uninfected explants (CC_{50}) *vs* the

249 EC_{50} values obtained on infected *ex vivo* splenic explants. The leishmanicidal effect of
250 AMB (drug in clinical use) was included as positive control just for comparison
251 purposes (Table 1, entry 14).

252 Two types of phosphorus substituted THQ and QUIN derivatives have been tested on
253 *Leishmania* parasites: i) substituted 1,2,3,4-tetrahydroquinolines (THQ, Chart 1, Table
254 1, entries 1 to 8) and ii) substituted derivatives of quinolines (QUIN, Chart 2, Table 1,
255 entries 9 to 13). In the case of 1,2,3,4-tetrahydroquinolinyl-phosphines **4** (Table 1,
256 entries 1 to 3) high antileishmanial activity on both intracellular amastigote form (EC_{50}
257 = 1.75 μM) and the free-living promastigotes (EC_{50} = 3.14 μM) was observed,
258 specifically in compound **4a** (Chart 1) that displays a fluorine atom at position 4 of the
259 aryl ring. Furthermore, this compound has low cytotoxic effect on non-infected
260 splenocytes, which confers it a good SI > 50. Similarly, it occurs with the
261 diphenylphosphines **4b** (Chart 1, Table 1, entry 2) and **4c** (Chart 1, Table 1, entry 3), but
262 in these cases the killing effect on promastigotes is much lower (EC_{50} = 20.91 μM for
263 entry 2, and EC_{50} = 27.72 μM for entry 3). In addition, the cytotoxic effect on
264 splenocytes for compounds **4b** and **4c** was higher and in consequence their SI lower (SI
265 = 26.2 and 8.6, respectively). It is noteworthy that these substituted phosphine
266 derivatives **4** consistently inhibited both LTopIB and hTopIB, this particular issue will
267 be discussed later.

268 A second group of phosphorus substituted THQ and QUIN compounds corresponds to
269 1,2,3,4-tetrahydroquinolinylphosphine sulfides **5** (Chart 1, Table 1, entries 4 and 5) and
270 quinolinylphosphine sulphides **7** (Chart 2, Table 1, entries 9 and 10). These compounds
271 were also tested on the transgenic cell strain of *L. infantum*-iRFP parasites. It is
272 remarkable that 1,2,3,4-tetrahydroquinoline compounds **5** containing the phosphine
273 sulfide group was very active killing intracellular amastigotes (EC_{50} = 0.61 μM and

EC_{50} = 2.73 μM for entries 4 and 5, respectively) unlike those derived from the quinoline ring **7** (EC_{50} > 10 μM in both cases). THQ **5a** was the most interesting compound of the series with a SI value of 56.87. The aromatic polycyclic compounds **7** did not show high cytotoxic values for splenocytes, all of them over 50 μM. However, since the effect on amastigote could not be accurately measured beyond 10 μM, the actual SI value for these compounds was not determined.

Finally, excellent results were observed for the phosphine oxides derived either from 1,2,3,4-tetrahydroquinolines **6** or quinolines **8** core rings. All of them were deadly for intracellular amastigotes at < 5 μM final concentration. Very interesting were the outcomes obtained with compounds **6b** (Chart 1, Table 1, entry 7) and **8b** (Chart 2, Table 1, entry 12), which are among the safest compounds used in the current study in terms of SI (43.6 and 51.1, respectively), and both displayed at least one fluorine atom in its structure. However, the presence of a naphthyl substituent in the quinoline ring did not improve the antileishmanial characteristic of compound **8a**.

Inhibition of leishmanial and human TopIB. With the aim of explaining the mechanism of action of the current series of compounds and based on the results reported previously, we have performed a series of experiments driven to inhibit recombinant LTopIB and hTopIB activities *in vitro*. In this regard, a conventional supercoiled plasmid relaxation assay was carried out based on the ability of these compounds to prevent the relaxation of supercoiled circular DNA mediated by TopIB.

A TopIB-deficient *Saccharomyces cerevisiae* platform was used to express recombinant *LTopIB* and *hTopIB* genes, which were purified as described elsewhere [58]. The effect of these compounds was compared with the inhibitory effect of CPT that was used as positive control in these experiments. Compounds were preincubated with the enzyme

298 at 37ºC during 15 min before the addition of supercoiled plasmid DNA and incubated
299 for increasing time periods (2 min, 4 min, 8 min and 16 min).

300 Equal concentrations of DMSO were added to each reaction in order to assess the
301 potential negative effect of the solvent. DNA relaxation products were then resolved by
302 electrophoresis in 1% agarose gels, stained with ethidium bromide and visualized under
303 UV lamp using a digital gel documentation system. Given that CPT does not bind the
304 enzyme in the absence of DNA, the preincubation step with CPT was unnecessary
305 [59,60].

306 From the results summarized in Table 2, it is noteworthy that the only compounds that
307 were consistently inhibitors of TopIB from both sources in time and concentration were
308 the 1,2,3,4-tetrahydroquinolinylphosphines **4** (entries 1 to 3). When LTopIB and
309 hTopIB were incubated at different concentrations of these compounds for a period of 5
310 min, dose/response curves were yielded that permitted us to calculate IC_{50} values
311 comprised between 23.6 to 84.5 μM, being **4c** the most active compound with IC_{50} =
312 23.64 ± 0.86 μM.

313 With the exception of compound **7a** (IC_{50} = 34.28 ± 0.91 on LTopIB and IC_{50} = 27.39 ±
314 0.47 μM on hTopIB, Chart 2, Table 2, entry 9), the second set of tetrahydroquinolinyl- **5**
315 and quinolinyl-phosphine sulfides **7** did not show the capacity to inhibit TopIB. Other
316 series distinct that present were recently tested on hTopIB with variable results. In such
317 a way, compound **7b** (Chart 2, Table 2, entry 10) that was tested previously, showed
318 weak inhibition on hTopIB at short time periods (< 3 min) [52]. We could not find any
319 inhibitory effect on both hTopIB and LTopIB for this compound for a period of 5 min.

320 Finally, from the series of tetrahydroquinolinyl- **6** and quinolinyl-phosphine oxides **8**,
321 only the compound **8c** (Chart 2, Table 2, entry 13), showed apparent inhibition of

TopIB (IC_{50} = 48.11 ± 0.33 μM on LTopIB and IC_{50} = 69.65 ± 1.29 μM on hTopIB), assayed at 5 min. In previous reports we showed the strong time-dependence of these compounds, assayed at a maximum of 3 min over hTopIB [52]. In our case, we did similar experiments and with exception of compound **8c** no inhibition at all was found for the phosphine oxides assayed [61].

Table 2. Inhibition of relaxation activity of LTopIB and hTopIB by phosphorus containing quinoline derivatives.

		Time (min)				Inhibition LTopIB	Inhibition hTopIB
entry	type	2	4	8	16	IC_{50} (μM)	IC_{50} (μM)
1	**4a**	+++	+++	+++	+++	54.21 ± 2.39	42.18 ± 1.76
2	**4b**	+++	+++	+++	+++	47.85 ± 0.38	44.79 ± 1.02
3	**4c**	+++	+++	+++	+++	23.64 ± 0.86	84.56 ± 2.07
4	**5a**	+++	+++	-	-	93.73 ± 3.47	n.i.
5	**5b**	-	-	-	-	n.i.	n.i.
6	**6a**	-	-	-	-	n.i.	n.i.
7	**6b**	-	-	-	-	n.i.	n.i.
8	**6c**	-	-	-	-	n.i.	n.i.
9	**7a**	+++	++	-	-	34.28 ± 0.91	27.39 ± 0.47
10	**7b**	-	-	-	-	n.i.	n.i.
11	**8a**	-	-	-	-	n.i.	n.i.
12	**8b**	-	-	-	-	n.i.	n.i.
13	**8c**	+++	+++	+++	-	48.11 ± 0.33	69.65 ± 1.29
CPT	-	+	-	-	-	n.i.	n.i.

[a]Compounds were preincubated with the enzyme for 15 min and then 0.5 μg supercoiled DNA was added. For time/course experiments and for dose/response experiments IC_{50} values are expressed as mean ± sd of three different experiments by triplicate

4. Computational analysis

Taking into account that theoretical calculations allowed the estimation of Molecular Electrostatic Potential Surface (MEPS), Highest Occupied – Lowest Unoccupied Molecular Orbital (HOMO-LUMO) energy gap and related parameters, which depicted the potential kinetic stability and reactivity of the target compounds [62], theoretical studies using Density Functional Theory (DFT) [63] involving the well-known Becke

three-parameter Lee-Yang-Parr function (B3LYP) [64] and 6-31G (d, p) level of theory for the synthesized compound were carried out.

4.1. Stereoelectronic properties. The molecular DFT-based parameters such as, electronic chemical potential (μ), chemical hardness (η), global electrophilicity (ω), maximum number of accepted electrons (ΔNmax) and Free energy in gas and in aqueous medium for compounds **4**-**8** are reported in Table 3. A large HOMO-LUMO gap represents a hard molecule while a small gap indicates a soft or more reactive/less stable molecule. Similarly, the global electrophilicity index (ω), a global reactivity index that is related to chemical hardness and chemical potential, represents the measure of the stabilization in energy achieved when the system acquires an additional electronic charge from the environment. Thus, tetrahydroquinolinyl phosphine derivatives **4**, are the most stable (Table 3), with the highest gap value, higher hardness and greater chemical potential than the rest of compounds and they are the least electrophilic, with the lowest dipolar moment. Among those 3 compounds, the compound **4c** (Chart 1), the one that best inhibits LTopIB (Table 2), presents the smallest hardness (which would imply a greater reactivity) and it is slightly less electrophilic.

Regarding tetrahydroquinolinyl- **5** and quinolinylphosphine sulfides **7** are more reactive than the compounds **4** of the former group, presenting gap values from 3.32 to 4.37 (Table 3). This last value corresponds to compound **5a** (Chart 1), which presents similar biological properties to those of compounds **4**. However, compounds **5b** (Chart 1), **7a** and **7b** (Chart 2) present globally smaller hardness with lower chemical potential and higher electrophilicity than compounds **4**. It is noteworthy that compound **5b** containing a nitro (NO_2) group, which presents the lowest biological activity, has a very high dipole moment (7.573 D) and is the most electrophilic.

Table 3. Calculated energies and molecular proprieties computed at B3LYP/6-31G** basis set level of theory for compounds **4** to **8**.

Compound	ΔG (g) (in a.u.)	ΔG (aq) (in a.u.)	E_{HOMO} (eV)	E_{LUMO} (eV)	Gap (-eV)	η (in a.u.)	μ (in a.u.)	ω (eV)	ΔN_{max} (in a.u.)	Dipole moment (debye)
4a	-1769.32634	-1769.33622	-0.19113	-0.02013	4.65	0.17100	-0.10563	0.032625	0.617719	1.455
4b	-1808.62328	-1808.63309	-0.19055	-0.01929	4.66	0.17126	-0.10492	0.032139	0.612636	1.599
4c	-1823.87801	-1823.88939	-0.1864	-0.01732	4.60	0.16908	-0.10186	0.030682	0.602437	1.570
5a	-2182.79925	-2182.81549	-0.19318	-0.0326	4.37	0.16058	-0.11289	0.039682	0.703014	4.690
5b	-2272.80606	-2272.82402	-0.20561	-0.08354	3.32	0.12207	-0.14458	0.085615	1.184361	7.573
6a	-1859.83221	-1859.84674	-0.18004	-0.02563	4.20	0.15441	-0.10284	0.034243	0.665987	1.889
6b	-2043.05448	-2043.06812	-0.19116	-0.03103	4.36	0.16013	-0.11110	0.038538	0.693780	4.636
6c	-1883.87588	-1883.88917	-0.18571	-0.02844	4.28	0.15727	-0.10708	0.036450	0.680836	3.777
7a	-2502.21758	-2502.23482	-0.20724	-0.07865	3.50	0.12859	-0.14295	0.079451	1.111634	7.081
7b	-2264.42140	-2264.43846	-0.20455	-0.07245	3.59	0.13210	-0.13850	0.072605	1.048448	5.691
8a	-1896.57537	-1896.59397	-0.20852	-0.06779	3.83	0.14073	-0.13816	0.067814	0.981703	4.769
8b	-1842.21196	-1842.229769	-0.22375	-0.06855	4.22	0.15520	-0.14615	0.068814	0.941688	3.819
8c	-2040.68809	-2040.705667	-0.22747	-0.07367	4.19	0.15380	-0.15057	0.073704	0.978999	5.941

Abbreviations: ΔG (g): Free energy in gas phase[a]; ΔG (aq): Free energy in aqueous medium[b];Gap: E_{HOMO}- $E_{LUMO;}$ η: Hardnesses[c]; μ:Chemical Potentials[c]; ω:Global Electrophilicities[c] and Δ*N*max: Maximun Number of Accepted Electrons[c].

[a] Computed a B3LYP(PCM)/6-31G**+ΔZPVE level; [b] Computed a B3LYP(PCM)/6-31G**+ΔZPVE level using water as solvent; [c]Computed at the B3LYP/6-31G** level of theory according to the approach and equations described previously.

Finally, the phosphine oxide derivatives **6** and **8**, except compound **8a** (Chart 2), are less stable than phosphine compounds **4**, but more stable than phosphine sulfide derivatives **5** and **7**. In general, they have lower hardness than phosphines **4**, but higher than phosphine sulfides **5** and **7**. Within this group, the tetrahydroquinolines **6** can be distinguished from the quinolines **8**. Compounds **6** present a lower dipole moment and are harder and less electrophilic than **8**. Among the aromatic compounds **8**, compound **8c** (Chart 2) stands out (greater inhibition of TopIB, in this group) that presents a high dipolar moment (5.941 D), is the most electrophilic of this group, and has the lowest chemical potential.

4.2. Molecular Electrostatic Potential Surface (MEPS) analysis. MEPS is a plot of electrostatic potential mapped on to constant potential electron density surface. These surfaces help in predicting reactivity sites towards positively and negatively charged reactants. MEP surfaces reveal the size shape and variation of electron density, electronegativity, partial charges and the sites of chemical reactivity within the molecule [62]. Figure 2 shows the MEPS of compounds **4**-**8**, that were calculated using DFT [63] with the standard basis set B3LYP/ 6-31G (d, p) level of theory. From these calculations it can be seen that tetrahydroquinolinyl phosphines **4** have a local negative electrostatic potential on the benzene ring of the bicyclic tetrahydroquinoline ring system. Furthermore, in the case of compound **4c** (Chart 1, Figure 2) due to the methoxy (OCH_3) group, a negative electrostatic potential appears on oxygen, greater than in the rest of the compounds of the tetrahydroquinolinyl phosphine group, even superior than that which appears on the fluorine (F) substituents of the compounds **4a** and **4b**. However, in the most biologically active compound **4a** local positive electrostatic potential appears over the hydrogens of the phenyl group in the 2 position of the quinoline ring. The potential values for these molecules, lower than for the rest, may

suggest that electrostatic interactions with the target may not be the most important factor in their biological activity. For the rest of the compounds the most negative electrostatic potential is located on the S atom (phosphine sulfides **5** and **7**, Scheme 1, *vide supra*) or on the O atom (phosphine oxides **6** and **8**, Scheme 1). In addition, the limits of electrostatic potential (Figure 2) for phosphine oxides are higher than in the case of phosphine sulfides. Regarding phosphine sulfides, compounds **5** and **7** (Figure 2) have negative electrostatic potential located on the sulfur atom. However, differences can be observed in other areas of the molecules. An excessively negative electrostatic potential appears on the nitro (NO_2) group of compound **5b** (Chart 1, Figure 2), while on the biologically active compound **5a** a positive electrostatic potential appears in the same area, in this case on the hydrogen atoms of the methoxy (OCH_3) group. As regards of quinolines **7**, in addition to the negative electrostatic potentials located on the sulfur atom, there are areas of negative values on the fluorine atoms of the trifluoromethyl (CF_3) group and fluorine of compound **7a** (Chart 2, Figure 2) and negative values on the F atoms of compound **7b** (Figure 2).

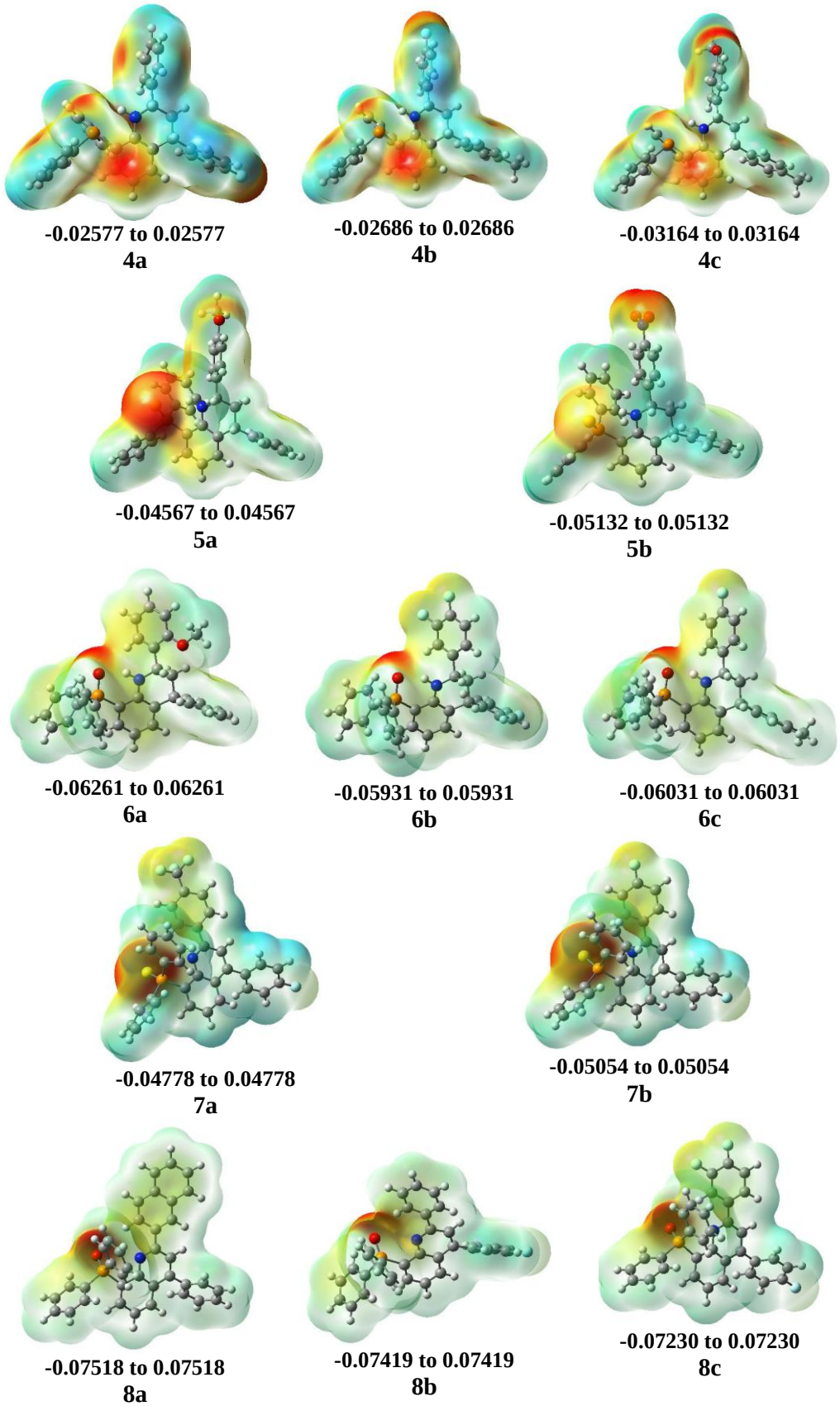

Figure 2. MEP surfaces mapped from total electron density for compounds **4** to **8**. Electrostatic potentials are displayed on a 0.002 a.u. isodensity surface. The limits of electrostatic potentials for each molecule are under surfaces. Potential increases in the following order: red (most negative)/orange/yellow/green/blue (most positive).

Finally, phosphine oxide compounds **6** and **8** (Figure 2) present the largest range of electrostatic potential. With the exception of compound **8a** (Chart 2), in addition to negative electrostatic potential located on oxygen atom of phosphine oxide group, they present other local negative electrostatic potentials mainly in the fluorine atoms, but the most biologically active compounds **6a**, **6b** and **8c** show local positive electrostatic potential areas. In the case of **6a** (Chart 1) on the hydrogen atoms of the methoxy group (Figure 2) and for **6b** (Chart 1) and **8b** (Chart 2) on the hydrogen atoms of the phenyl group located in the position 2 of the quinoline ring next to the two fluorine toms (Figure 2). It is noteworthy that the values of the potentials for these compounds higher than the other ones indicate that the electrostatic interactions would be more efficient than in the other molecules.

4.3. Docking studies. Among all the compounds synthesized in this work, a molecular docking study of those who showed inhibition of TopIB was carried out to investigate its plausible binding pattern and its interaction with the key amino acids and DNA nucleobases in the active site of the enzyme. Since a complete crystallographic model of LTopIB with CPT is not available, our docking studies of compounds **4a**-**c**, **7b** and **8c**, in the CPT binding site were done using the CPT−hTopIB−DNA ternary complex (PDB ID: 1T8I) [65], as template using the graphical interface Maestro [66] and Glide 6.9 [67] in XP (extra-precision) mode [68]. The pose/position with the highest score was retained in the workspace for detailed evaluation of the ligand binding. A comparative analysis of the mode of union of different types of inhibitors of Top IB indicates [62,69] that all of them are located in the catalytic center of hTopIB, intercalated between the DNA nucleobases, near Arg 364. This residue is located, together with Asp 533 and Phe 361, in the cavity of the minor groove of the DNA, in the zone of rupture. In addition, the major groove cavity in the excision zone is limited by residues Glu 356, Asn 352,

Pro 431, Lys 751 and Asn 722, this latter neighboring to catalytic Tyr 723. Some of the inhibitors direct their substituents towards the side chain of Asn 352, which has a high mobility (according to molecular dynamics simulations), which makes this residue to play a key role in the modulation of drug binding [70].

In our case, the most important evaluation criterion was the observation of whether the ligands were located between C112-TGP11 and A113-T10 nucleobases, where the DNA rupture site is located, avoiding the re-ligation of such bases, according to the concept of interfacial inhibition proposed by Pommier [71].

The formation of hydrogen bonds with important residues and the existence of hydrophobic interactions with hTopIB residues and DNA, were also taken into account. Likewise, based on the above interactions, the obtained values from the gscore parameters (score, punctuation) indicate the virtual affinity of the ligands to the complex, and gemodel, which is the theoretical value of the interaction energy of the ligand with the hTopIB/DNA complex, were considered (Table 4).

Table 4. gscore and gemodel values for best hTopIB inhibitors.

Entry	Compound	gscore (kcal/mol)	gemodel (kcal/mol)
1	**4a**	-6.581	-85.955
2	**4b**	-6.238	-84.305
3	**4c**	-8.699	-78.582
4	**7a**	-8.385	-116.768
5	**8c**	-9.297	-105.950

In the case of tetrahydroquinolinylphosphines **4a-c** (Chart 1) two different orientations could be observed (Figures 3A, 3B and 4A, 4B). Compounds **4a** and **4b**, with a low value of gscore (Table 4, entries 1 and 2), are stacked between nucleobases in the rupture zone, where π-π stacking interactions of one of the phenyl rings bounded to the phosphorus atom and the aromatic ring of the tetrahydroquinoline skeleton can be observed. In addition, the substituent at position 4 of tetrahydroquinoline skeleton is

459 oriented towards the minor groove presenting hydrophobic interactions with Phe 361
460 and Ile 420, while the substituent at position 2 is oriented towards the major groove,
461 showing hydrophobic interactions with Ile 355, Trp 416 and Ile 427 (Figures 3A, 3B
462 and 4A, 4B).
463 However, another orientation pattern is observed for tetrahydroquinolinylphosphine **4c**
464 (which presents the highest gscore of the phosphines **4**, see Table 4 entry 3). Only the
465 substituent at position 4 is oriented towards the minor groove, establishing π-π stacking
466 interactions with the bases TGP11 and DA113 (Figures 3C and 4C). Moreover, the
467 aromatic substituent at position 2, with a methoxyl group, is located close to Glu 356,
468 presenting π-π stacking interactions with DA113. While the two phenyl substituents of
469 the phosphine group are oriented towards the major groove presenting hydrophobic
470 interactions with Ile 424, Tyr 426, Ile 427, Ala 351, Met 426 and Leu 429.

471 With respect to quinolinylphosphine sulfide **7a** (Chart 2), which presents the highest
472 interaction energy gemodel (Table 4), it is placed parallel to the DNA nucleobases,
473 being established π-π stacking interactions between the quinoline ring and TGP11 and
474 the phenyl substituent at position 2 with TGP11 and DA113 (Figure 3D). The
475 substituent at position 4 is oriented towards the minor groove, while that one in position
476 2 is oriented towards the major groove. One of the phenyl substituents of phosphine
477 sulfide interacts hydrophobically with Pro 431 (Figures 3D and 4D).

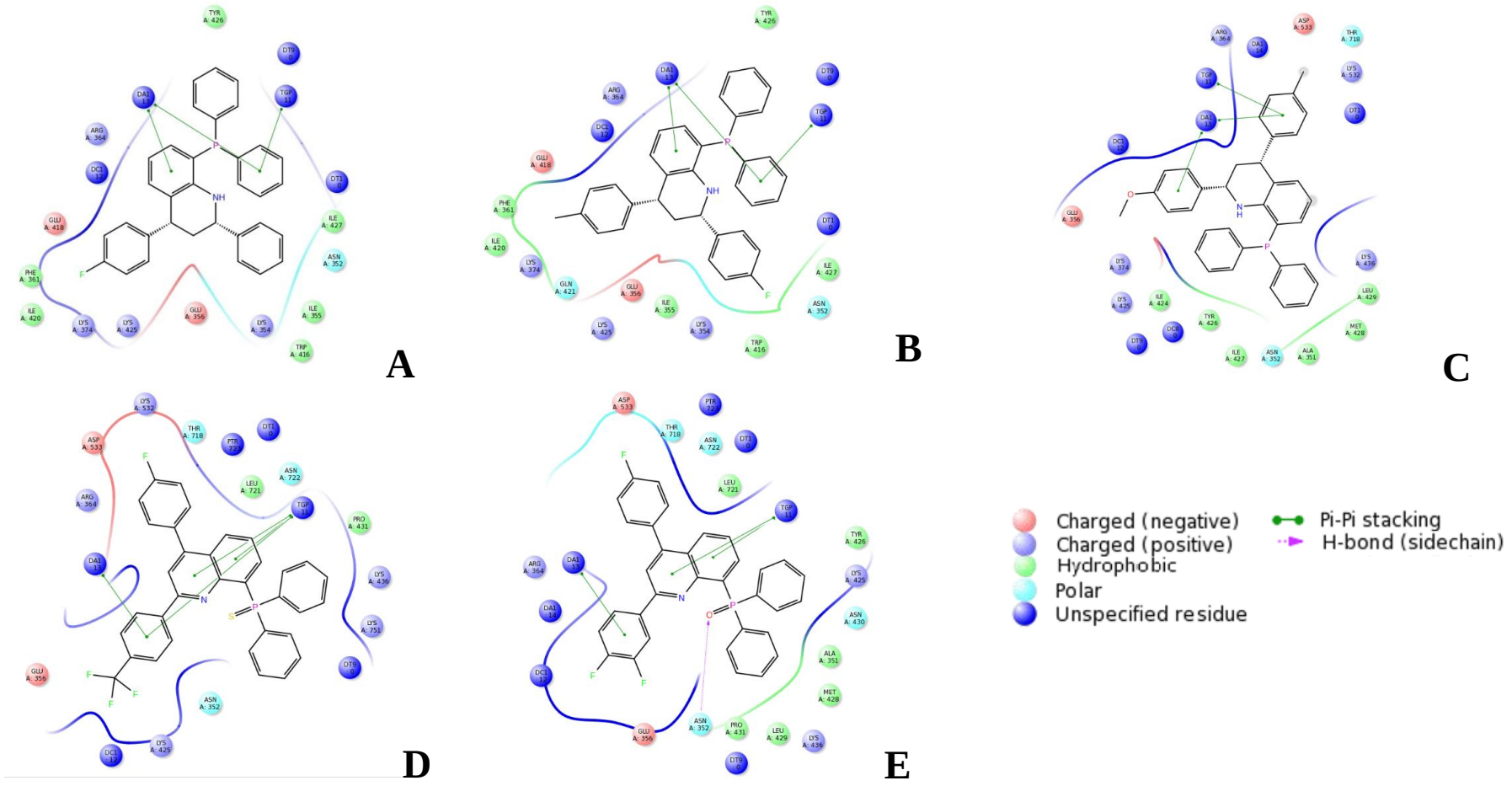

Figure 3. The 2D interaction of compounds **4a** (A), **4b** (B), **4c**(C), **7a** (D) and **8c** (E) in the binding site of hTop1B. (For interpretation of the references to colour in this figure legend, the reader is referred to the web version of this article).

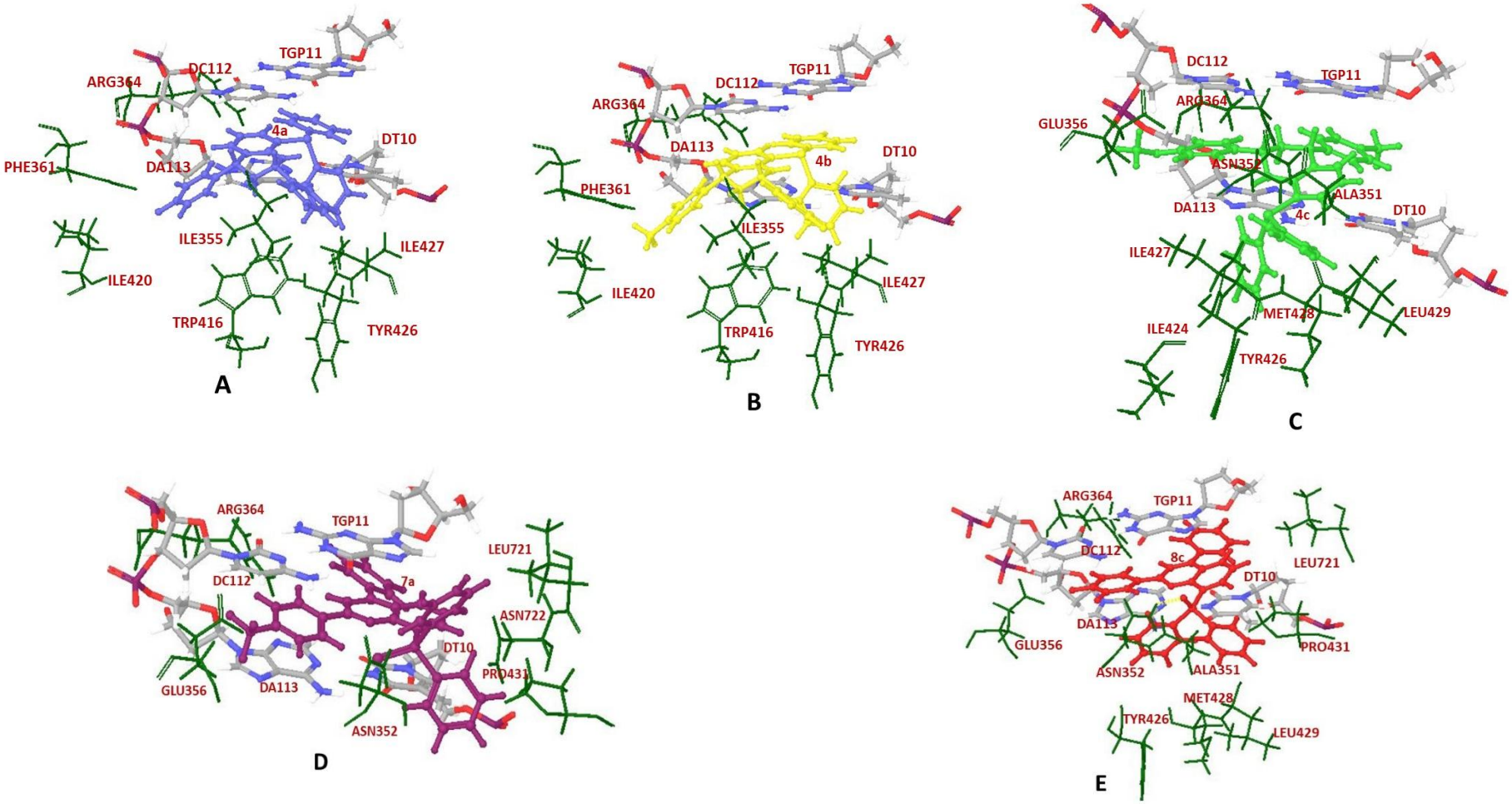

Figure.4. The potential binding modes of compounds **4a** (A, in blue), **4b** (B in yellow), **4c** (C in lime green), **7a** (D in purple) and **8c** (E in red) with hTop1B (PDB code: 1T8I). The key residues of the protein were colored in dark green, and DNA bases by the atom type. The hydrogen bond for **8c** (in E) was shown with yellow dashed line. (For interpretation of the references to colour in this figure legend, the reader is referred to the web version of this article).

Finally, quinolinylphosphine oxide **8c** (Chart 2), the compound with the highest value of gscore (Table 4, entry 5), is located at the cleavage site parallel to the DNA nucleobases with the substituent at position 4 oriented towards the minor groove (Figure 3E). Alternatively, the diphenylphosphine oxide group is directed towards the major groove, establishing π-π stacking interactions between the quinoline ring and TGP11 and the difluorinated ring of position 2 with DA113. The two aromatic substituents of the phosphine oxide group are oriented towards the major groove giving hydrophobic interactions with Pro 431, Leu 429, Met 428, Ala 351 and Tyr 426. Furthermore, in this case, the oxygen of the phosphine oxide group forms a hydrogen bond with one of the hydrogens of the amide group of Asn 352 (Figures 3E and 4E).

4.4. Predictive druggability analysis. Compounds with best leishmanicidal activity and weak cytotoxic effect on mouse macrophages (SI > 30) were submitted to *in silico* pharmacokinetic properties prediction. To predict the druggability of the selected hits, we analysed the parameters included in Table 1 of Supporting Material, provided by http://www.swissadme.ch/index.php and admetSAR (http://www.admetexp.org/) servers, both freely accessible web-based applications. Despite the good SI of the chosen compounds their druggability was compromised because, with exception of compounds **4a** and **8b** (MW 487.55 and 499.51), the rest of the compounds violated two statements of Lipinski's rule – size (≤ 500 Da) and cLogP (≤ 4.15) – but showed acceptable number of Rotatable Bonds (n-ROTB) values (≤10). However, despite of that, the predicted HIA (human intestinal absorption) and Caco2 absorbability were positive for all compounds. In the case of metabolism, the compounds selected in Table 1 (Supporting Material) showed different predicted patterns of interaction with CYP450 but all of them had high enzyme promiscuity. Since CYP-mediated metabolism represents a major route of elimination of many drugs those compounds that are

substrate of CYP450 can be more readily removed that those that are not. From the results of Table 1 (Supporting Material), just compound **5a**, **6a** and **6b** are substrate of CYP450 subfamily 3A4, whereas most of them acted as inhibitors. In terms of predicted toxicity, the subtituted phosphine **4a** (Table 1, entry 1) was detected as potential mutagenic toxic with respect to the AMES test but none of them had predicted carcinogenic effects.

5. Conclusions

In conclusion, a wide range of hybrid phosphorated THQ and QUIN has been prepared by using the multicomponent Povarov reaction. The synthesis of these functionalized THQ containing phosphorus substituents, such as phosphines **4**, phosphine sulfides **5** and phosphine oxides **6**, involves the multicomponent aza-Diels-Alder reaction of aldehydes **1** with functionalized anilines **2**, and styrenes **3**. Subsequent dehydrogenation of 1,2,3,4-tetrahydroquinoline-phosphine sulfides **5** and - phosphine oxides **6** produced the corresponding quinolinyl-phosphine sulfides **7** and -phosphine oxides **8**.

After the preparation, their antileishmanial activity on promastigotes and amastigote-infected splenocytes of *L. infantum* has been evaluated. In general, not only functionalized THQ **4-6**, but also phosphorated QUIN **7** and **8** have shown higher antiparasitic activity on intracellular amastigotes than on free-living promastigotes. Good antileishmanial activity of functionalized THQ **4a**, **5a, 6b** and QUIN **8b** has been observed with similar activity than the standard drug amphotericin B (AMB) and close selective index (SI between 43 and 57) towards *L. infantum* amastigotes to amphotericin B. Remarkably, the tetrahydroquinolylphosphine sulfide **5a** with electron-donating substituent (methoxy group) in *para* position of aromatic ring at position 2 of quinoline

system shows an EC_{50} value (0.61 ± 0.18 μM) similar to the standard drug amphotericin B (0.32 ± 0.05 μM) and similar selective index (SI = 56.87).

Regarding inhibition of LTopIB and hTopIB enzymatic activity, 1,2,3,4-tetrahydroquinolinylphosphines **4** were consistently inhibitors of TopIB from both sources in time and concentration, being **4c** the most active compound with IC_{50} = 23.64 ± 0.86 μM on leishmanial TopIB. And among QUIN derivatives **7** and **8**, only quinolinylphosphine sulphide **7a** (with a CF_3 group and a fluorine atom as substituents) inhibited LTopIB activity, but without selectivity on this enzyme respect to hTopIB.

Evaluation of the designed hybrid compounds based on their physicochemical properties has indicated that they are promising drug candidates with drug-like pharmacotherapeutic profiles. In addition, the stereoelectronic properties such as HOMO (highest occupied molecular orbital), LUMO (lowest unoccupied molecular orbital), and MEP (molecular electrostatic potential) surfaces calculated by quantum chemical methods provided insight on the possible binding mode of the most active compounds within an allosteric site.

Some of the compounds that we presented for the first time in this manuscript were inhibitors of the relaxation of the supercoiled DNA mediated by TopIB with an effect both dependent on concentration and time, and showed an estimable efficacy against the intracellular forms of *L. infantum* at micromolar concentrations, as well as a SI > 50. This was the case of the compounds derived from 1,2,3,4-tetrahydroquinolinylphosphine **4a** with a value of EC_{50} of 1.75 ± 0.51 μM as well as for 1,2,3,4-tetrahydroquinolinylphosphine sulfide **5a** with an EC_{50} value of 0.61 ± 0.18 μM and the sulfide of quinolinylphosphine **8b** with an EC_{50} value of 1.39 ± 1.08 μM. In addition, the antileishmanial activity of some of them could be explained partly by the

inhibition of the TopIB, although it could only be explained as a secondary role in their biological efficacy.

Nevertheless, the strong antileishmanial activity and the relative safety of many of the present compounds provide a promising basis for further development of biologically active phosphorus quinoline derivatives.

6. Experimental protocols

6.1 Chemistry

6.1.1. General experimental information

All reagents from commercial suppliers were used without further purification. All solvents were freshly distilled before use from appropriate drying agents. All other reagents were recrystallized or distilled when necessary. Reactions were performed under a dry nitrogen atmosphere. Analytical TLCs were performed with silica gel 60 F_{254} plates. Visualization was accomplished by UV light. Column chromatography was carried out using silica gel 60 (230-400 mesh ASTM). Melting points were determined with a digital melting point apparatus without correction. NMR spectra were obtained on a 300 MHz and on a 400 MHz spectrometers and recorded at 25 ºC. Chemical shifts for ^{1}H NMR spectra are reported in ppm downfield from TMS, chemical shifts for ^{13}C NMR spectra are recorded in ppm relative to internal chloroform (δ = 77.2 ppm for ^{13}C), chemical shifts for ^{19}F NMR are reported in ppm downfield from fluorotrichloromethane ($CFCl_3$). Coupling constants (*J*) are reported in Hertz. The terms m, s, d, t, q refer to multiplet, singlet, doublet, triplet, quartet. ^{13}C NMR, and ^{19}F NMR were broadband decoupled from hydrogen nuclei. High resolution mass spectra (HRMS) was measured by positive-ion electrospray ionization (EI) method using a mass spectrometer Q-TOF. Compounds **2a**, **2b**, **4a-c**, **5a, 5b** and **7a** were prepared as

previously described [54]. Compounds **6a** and **7b** were prepared as previously described [52].

6.1.2. Compounds Purity Analysis

All synthesized compounds were analyzed by HPLC to determine their purity. The analyses were performed on Agilent 1260 infinity HPLC system (Chiracel-IC column, 3μm, 0.46 cm×25 mm) at room temperature. All the tested compounds were dissolved in dichloromethane, and 5μL of the sample was loaded onto the column. Ethanol and heptane were used as mobile phase, and the flow rate was set at 1.0 mL/min. The maximal absorbance at the range of 190−400 nm was used as the detection wavelength. The purity of all the tested compounds is >95%, which meets the purity requirement by the Journal.

6.1.3. ***1,2,3,4-tetrahydroquinolinylphosphines 4 and 1,2,3,4-tetrahydroquinolinylphosphine sulfides 5***

6.1.3.1. ***8-(Diphenylphosphanyl)-2-phenyl-4-(4-fluorophenyl)-1,2,3,4-tetrahydroquinoline*** **(4a)**. The compound was prepared and characterized as previously described [54]. Purity 99.19 % (EtOH/Heptane = 10/90, Rt = 6.627 min).

6.1.3.2. ***8-(Diphenylphosphanyl)-2-phenyl-4-(4-methylphenyl)-1,2,3,4-tetrahydroquinoline*** **(4b)**. The compound was prepared and characterized as previously described [54]. Purity 99.14 % (EtOH/Heptane = 10/90, Rt = 6.160 min).

6.1.3.3. ***8-(Diphenylphosphanyl)-2-(4-methoxyphenyl)-4-(4-methylphenyl)-1,2,3,4-tetrahydroquinoline*** **(4c)**. The compound was prepared and characterized as previously described [54]. Purity 97.39 % (EtOH/Heptane = 10/90, Rt = 4.422 min).

6.1.3.4. ***8-(Diphenylphosphinosulfide)-2-(4-methoxyphenyl)-4-phenyl)-1,2,3,4 tetrahydroquinoline*** **(5a)**. The compound was prepared and characterized as previously described [54]. Purity 98.47 % (EtOH/Heptane = 10/90, Rt = 6.823 min).

6.1.3.5. ***8-(Diphenylphosphinosulfide)-2-(4-nitrophenyl)-4-phenyl)-1,2,3,4-tetrahydro-quinoline*** **(5b)**. The compound was prepared and characterized as previously described [54]. Purity 96.00 % (EtOH/Heptane = 10/90, Rt = 5.043 min).

6.1.3.6. ***8-(Diphenylphosphinosulfide)-2-(4-trifluorophenyl)-4-(4-fluorophenyl)-quinoline*** **(7a).** The compound was prepared and characterized as previously described [54]. Purity 96.08 % (EtOH/Heptane = 10/90, Rt = 5.871 min).

6.1.3.7. ***(2,4-Bis(4-fluorophenyl)quinolin-8-yl)diphenylphosphine sulfide*** **(7b**). The compound was prepared and characterized as previously described [52]. Purity 97.58 % (EtOH/Heptane = 10/90, Rt = 3.42 min).

6.1.4. **Synthesis of 1,2,3,4-tetrahydroquinolinylphosphine oxides 6 or quinolinylphosphine oxides 8 by Povarov reaction.**

6.1.4.1. **General procedure.** A mixture of (2-Aminophenyl)diphenylphosphanoxide **2c** (10 mmol, 2.933 g), freshly distilled aldehyde **1** (10 mmol), styrene **3** (12 mmol) and 1 equivalent of $BF_3 \cdot Et_2O$ (10 mmol, 1.230 mL) in $CHCl_3$ (25 mL) and in the presence of molecular sieves (4Å), was stirred and heated at reflux until TLC, ^{31}P NMR and ^{1}H NMR analysis indicated the consumption of starting materials. The molecular sieves were removed by filtration and the resulting solution was diluted with methylene chloride (50 mL), washed with a solution of NaOH 2M (50 mL) and water (50 mL), extracted with methylene chloride (2 x 20 mL), and dried over anhydrous $MgSO_4$. Removal of solvent under vacuum led to a solid that was purified by flash column

chromatography on silica gel using a gradient of elution of 5-70% ethyl acetate in hexane to afford products **6** or **8.**

6.1.4.1.1. ***(2-(2-Methoxyphenyl)-4-phenyl-1,2,3,4-tetrahydroquinolin-8-yl)diphenylphosphine oxide*** (**6a**). The compound was prepared and characterized as previously described [52]. Purity 98.19 % (EtOH/Heptane = 10/90, Rt = 4.636 min).

6.1.4.1.2. ***2-(3,4-Difluorophenyl)-4-(4-fluorophenyl-1,2,3,4-tetrahydroquinolin-8-yl)diphenylphosphine oxide*** (**6b**). The general procedure was followed using 3,4-difluorobenzaldehyde (10 mmol, 1.072 mL) and 4-fluorostyrene **3b** (12 mmol, 1.437 mL), heated to reflux for 48 h affording compound **6b** (3.073 g, 57 %) as a white solid, mp 167-169 ºC (ethyl acetate/hexane). ^{1}H NMR (400 MHz, $CDCl_3$) δ: 1.72 (s, 1H, NH), 1.88 (ddd, $^{2}J_{HH}$ = 11.7 Hz, $^{3}J_{HH}$ = 11.7 Hz, $^{3}J_{HH}$ = 11.4 Hz, 1 H, CH_2), 2.15-2.20 (m, 1 H, CH_2), 4.21 (dd, $^{3}J_{HH}$ = 11.7 Hz, $^{3}J_{HH}$ = 4.6 Hz, 1 H, HC), 4.67 (dd, $^{3}J_{HH}$ = 11.7 Hz , $^{3}J_{HH}$ = 3.4 Hz ,1 H, HC), 6.40 (ddd, *J* = 10.4 Hz, *J* = 7.5 Hz, *J* = 3.0 Hz, 1 H), 6.64-7.14 (m, (m, 9 H), 746-7.77(m, 10 H) ppm; ^{13}C NMR {H} (75 MHz, $CDCl_3$) δ:41.1 (CH_2), 43.9 (CH), 55.9 (CH), 111.8 (d, $^{1}J_{CP}$ = 103.7 Hz, C), 114.9 (d, $^{2}J_{CF}$ = 17.7 Hz, HC), 115.4 (d, $^{3}J_{CP}$ = 13.6 Hz, HC), 115.7 (d, $^{3}J_{CP}$ = 20.2 Hz, 2 HC), 117.3 (d, $^{2}J_{CF}$ = 17.7 Hz, HC), 121.1 (HC), 125.7 (C), 128.6-133.3 (m, 14 HC and 2 C), 139.6 (C), 141.0 (C), 149.4 (dd, $^{1}J_{CF}$ = 246.5 Hz, $^{2}J_{CF}$ = 12.7 Hz, C-F) 149.7 (C), 150.5 (dd, $^{1}J_{CF}$ = 247.6 Hz, $^{2}J_{CF}$ = 12.8 Hz, C-F), 161.8 (d, $^{1}J_{CF}$ = 243.4 Hz, C-F) ppm; ^{31}P NMR (120 MHz, $CDCl_3$) δ: 36.38 ppm; ^{19}F NMR (282 MHz, $CDCl_3$) δ: -116.3 to -116.4 (m), -137.6 to -137.8 (m), -140.2 to -140.3 (m) ppm. HRMS (EI): calculated for $C_{33}H_{25}F_3NPO$ [M]+ 539.1626; found 539.1639. Purity 96.40 % (EtOH/Heptane = 10/90, Rt = 6.023 min).

6.1.4.1.3. ***2-(4-Fluorophenyl)-4-(4-methylphenyl-1,2,3,4-tetrahydroquinolin-8-yl)diphenylphosphine oxide*** (**6c**). The general procedure was followed using 4-

650 fluorobenzaldehyde (10 mmol, 1.079 mL) and 1-methyl-4-vinylbenzene **3c** (12 mmol,
651 1.575 mL), heated to reflux for 36 h affording compound **6c** (3.675 g, 71 %) as a white
652 solid, mp 207-209 ºC (ethyl acetate/hexane). ^{1}H NMR (400 MHz, $CDCl_3$) δ: 1.93 (ddd,
653 $^{2}J_{HH}$ = 12.7 Hz, $^{3}J_{HH}$ = 12.7 Hz, $^{3}J_{HH}$ = 11.5 Hz, 1 H, CH_2), 2.18 (ddd, $^{2}J_{HH}$ = 12.7 Hz,
654 $^{3}J_{HH}$ = 4.7 Hz, $^{3}J_{HH}$ = 3.4 Hz, 1 H, CH_2), 2.34 (s, 3 H, CH_3), 4.18 (dd, $^{3}J_{HH}$ = 12.7 Hz,
655 $^{3}J_{HH}$ = 4.7 Hz, 1 H, HC), 4.69 (dd, $^{3}J_{HH}$ = 11.5 Hz , $^{3}J_{HH}$ = 3.4 Hz ,1 H, HC), 6.36 (ddd,
656 *J* = 10.4 Hz, *J* = 7.6 Hz, *J* = 3.0 Hz, 1H), 6.81-7.15. (m, 11 H, NH and H), 7.44-7.78 (m,
657 10 H) ppm; ^{13}C NMR {H} (75 MHz, $CDCl_3$) δ: 21.22 (CH_3), 41.2 (CH_2), 44.3 (CH),
658 56.3 (CH), 111.0 (d, $^{1}J_{CP}$ = 105.0 Hz, C), 114.9 (d, $^{3}J_{CP}$ = 13.1 Hz, HC), 115.3 (d, $^{3}J_{CF}$ =
659 21.3 Hz, 2 HC), 126.3 (d, $^{3}J_{CP}$ = 7.5 Hz, C), 127.6-129.5 (m, 12 HC), 131.8-133.5 (m, 6
660 HC and 2 C), 136.5 (C), 139.8 (C), 141.1 (C), 149.9 (C), 162.0 (d, $^{1}J_{CF}$ = 243.8 Hz, $^{2}J_{CF}$
661 = 12.7 Hz, C) ppm; ^{31}P NMR (120 MHz, $CDCl_3$) δ: 35.47 ppm; ^{19}F NMR (282 MHz,
662 $CDCl_3$) δ: -116.1 to -116.3 (m), ppm. HRMS (EI): calculated for $C_{34}H_{29}FNPO$ [M]+
663 517.1971; found 517.1982. Purity 97.18 % (EtOH/Heptane = 10/90, Rt = 5.582 min).

664 *6.1.4.1.4.* ***Diphenyl(2-(naphthalen-2-yl)-4-phenyl quinolin-8-yl)phosphine oxide*** (**8a**).
665 The general procedure was followed using 2-naphthaldehyde (10 mmol, 1.072 mL) and
666 styrene **3a** (12 mmol, 1.374 mL), heated to reflux for 48 h affording compound **8a**
667 (4.359 g, 82 %) as a white solid, mp 236-238 ºC (ethyl acetate/hexane). ^{1}H NMR (400
668 MHz, $CDCl_3$) δ: 7.18 (bs, 5 H), 7.24-7.49 (m, 10 H), 7.52-7.68 (m, 3 H), 7.76 (dd, $^{3}J_{HH}$
669 = 8.4 Hz, $^{4}J_{HH}$ = 1.4 Hz, 1 H), 7.87-7.91 (m, 5 H), 8.07 (d, $^{3}J_{HH}$ = 8.4,), 8.60 (bs, 1 H),
670 ppm; ^{13}C NMR {H} (75 MHz, $CDCl_3$) δ: 119.8 (HC), 125.3-135.1 (m, 6 C and 24 HC),
671 136.2 (C), 138.2 (d, $^{3}J_{CP}$ = 9.0 Hz, HC), 144.8 (C) 148.4 (d, $^{2}J_{CP}$ = 5.2 Hz, C), 149.8 (C),
672 155.9 (C) ppm; ^{31}P NMR (120 MHz, $CDCl_3$) δ: 29.13 ppm. HRMS (EI): calculated for

673 $C_{37}H_{26}NPO$ [M]+ 531.1752; found 531.1754. Purity 95.73% (EtOH/Heptane = 10/90,
674 Rt = 9.909 min).

675 *6.1.4.1.5.* ***(4-(4-Fluorophenyl)-2-phenylquinolin-8-yl)diphenylphosphine oxide*** (**8b**).
676 The general procedure was followed using benzaldehyde (10 mmol, 1.016 mL) and 4-
677 fluorostyrene **3b** (12 mmol, 1.437 mL), heated to reflux for 48 h affording compound
678 **8b** (4.246 g, 85 %) as a white solid, mp 193-195 ºC (ethyl acetate/hexane). ^{1}H NMR
679 (400 MHz, $CDCl_3$) δ: 7.17-7.52 (m, 16 H), 7.64 (ddd, $^{3}J_{HH}$ = 9.3 Hz, $^{3}J_{HH}$ = 7.1 Hz, $^{4}J_{HP}$
680 = 1.3 Hz, 1 H), 7.76 (s, 1 H), 7.93 (dd, $^{3}J_{HH}$ = 7.1 Hz, $^{4}J_{HP}$ = 1.3 Hz, 4 H), 8.07 (dd, $^{3}J_{HH}$
681 = 8.4 Hz, $^{4}J_{HH}$ = 1.4 Hz, 1 H), 8.64 (ddd, $^{3}J_{PH}$ = 13.6 Hz, $^{3}J_{HH}$ = 7.2 Hz, $^{4}J_{HH}$ = 1.3 Hz, 1
682 H) ppm; ^{13}C NMR {H} (75 MHz, $CDCl_3$) δ: 115.9 (d, $^{2}J_{CF}$ = 21.5 Hz, 2 HC), 119.4
683 (HC), 126.0 (d, $^{2}J_{CP}$ = 7.7 Hz, C), 126.2 (d, $^{2}J_{CP}$ = 12.8 Hz, HC), 127.7-134.8 (m, 18 HC
684 and C), 134.0 (d, $^{4}J_{CF}$ = 3.2 Hz, C), 134.1 (d, $^{1}J_{CP}$ = 108.4 Hz, 2 C), 138.1 (d, $^{3}J_{CP}$ = 7.2
685 Hz, HC), 138.6 (C), 148.2 (d, $^{2}J_{CP}$ = 5.6 Hz, C), 148.6 (C), 155.9 (C), 163.2 (d, $^{1}J_{CF}$ =
686 247.8 Hz, C-F), ppm; ^{31}P NMR (120 MHz, $CDCl_3$) δ: 28.8 ppm; ^{19}F NMR (282 MHz,
687 $CDCl_3$) δ: -113.1 to -113.2 (m), ppm. HRMS (EI): calculated for $C_{33}H_{23}FNPO$ [M]+
688 499.1501; found 499.1503. Purity 98.68 % (EtOH/Heptane = 10/90, Rt = 9.698 min).

689 *6.1.5.* **Dehydrogenation of *2-(3,4-difluorophenyl)-4-(4-fluorophenyl-1,2,3,4-***
690 ***tetrahydroquinolin-8-yl)diphenylphosphine oxide* (6b) to *2-(3,4-difluorophenyl)-4-(4-***
691 ***fluorophenyl)quinolin-8-yl)diphenylphosphine oxide* (8c).** To a solution of the
692 tetrahydroquinoline **6b** (1 mmol, 0.539 g) in $CHCl_3$ (7 mL) was added DDQ (0.545 g, 2
693 mmol), and the mixture was heated to reflux for 2 h. The removal of the solvent under
694 vacuum afforded and oil, diethyl ether was added, and the resulting solid was removed
695 by filtration. The filtrate was removed under vacuum and the crude solid was purified
696 by recrystallization on ether to afford **8c** (0.530 g, 99 % yield) as a white solid m.p. 273-

275 °C (ethyl acetate/hexane). ^{1}H NMR (400 MHz, $CDCl_3$) δ: 7.04-7.14 (m, 3 H), 7.39-7.52 (m, 10 H), 7.63 (ddd, $^{3}J_{HH}$ = 8.4 Hz, $^{3}J_{HH}$ = 7.1 Hz, $^{4}J_{HP}$ = 1.3 Hz, 1 H), 7.68 (s, 1 H), 7.86-7.92 (m, 4 H), 8.06 (ddd, $^{5}J_{PH}$ = 2.6 Hz, $^{3}J_{HH}$ = 8.4 Hz, $^{4}J_{HH}$ = 1.2 Hz, 1 H), 8.49 (ddd, $^{3}J_{PH}$ = 14.1 Hz, $^{3}J_{HH}$ = 7.1 Hz, $^{4}J_{HH}$ = 1.4 Hz, 1 H) ppm; ^{13}C NMR {H} (75 MHz, $CDCl_3$) δ: 116.1 (d, $^{2}J_{CF}$ = 21.6 Hz, 2 HC), 116.9 (d, $^{2}J_{CF}$ = 18.3 Hz, HC), 117.4 (d, $^{2}J_{CF}$ = 18.3 Hz, HC), 118.9 (HC), 123.6 (HC), 126.2-135.7 (m, 6 C and 15 HC), 138.3 (HC), 148.3 (C), 149.1 (C), 150.6 (dd, $^{1}J_{CF}$ = 248.4 Hz, $^{2}J_{CF}$ = 12.9 Hz, C-F), 151.4 (dd, $^{1}J_{CF}$ = 251.3 Hz, $^{2}J_{CF}$ = 13.5 Hz, C-F), 153,7 (C), 163.2 (d, $^{1}J_{CF}$ = 248.9 Hz, C-F) ppm; ^{31}P NMR (120 MHz, $CDCl_3$) δ: 28.6 ppm; ^{19}F NMR (282 MHz, $CDCl_3$) δ: -112.7 to -112.8 (m), -136.4 to -136.6 (m), -137.3 to -137.6 (m) ppm. HRMS (EI): calculated for $C_{33}H_{21}F_3NPO$ [M]+ 535.1313; found 535.1395. Purity 99.60 % (EtOH/Heptane = 10/90, Rt = 9.603 min).

6.2. Biology

All protocols described in this work were approved by the Animal Care Committee of University of Leon, project license PI12/00104. It complies with European Union Legislation (2010/63/UE) and Spanish Act (RD 53/2013).

6.2.1. In vitro L. infantum promastigotes assays

The antiparasitic activity of the newly synthesized compounds against was assessed against a transgenic strain of *L infantum* BCN 150 that constitutively express the *irfp* gene encoding the infrared iRFP protein. The resulting *iRFP-L. infantum* strain, allows the detection of viable parasites in both promastigote and amastigote forms by measuring the emission of near infrared fluorescence [56]. The free-living promastigotes were cultured using M199 medium (Gibco), supplemented with 25 mM 4-(2-hydroxyethyl)-1-piperazineethanesulfonic acid (HEPES) pH 6.9, 7.6 mM hemin,

10 mM glutamine, 0.1 mM adenosine, 0.01 mM folic acid, 1xRPMI 1640 vitamin mix (Sigma), 10% (v/v) heat inactivated foetal bovine serum (Gibco), 50 U/mL penicillin and 50 µg/mL streptomycin. The antiproliferative effect of the compounds on promastigotes were assessed in 96-well optical bottom black plates (Thermo Scientific) seeded at a cell density of 1 x 10^6 cells/mL in the presence and absence of different concentrations of compounds incubated for 72 h. Both controls and treated groups were tested with DMSO concentrations below 0.1 %. The viability of promastigotes was assessed by measuring their fluorescence at 708 nm in an Odyssey (Li-Cor) infrared imaging system. Cell viability was used to determine the 50% effective concentration of promastigotes (EC_{50}). All compounds and controls were assayed by triplicate.

6.2.2. Ex vivo murine splenic explant cultures

BALB/c mice infected 5 weeks earlier with metacyclic promastigotes from iRFP *L.* infantum were sacrificed to extract the spleens, which were processed to obtain a suspension of primary splenocytes. Briefly, freshly dissected spleens were washed with cold phosphate-buffered saline (PBS), cut in small pieces and incubated with 5 mL of 2 mg/mL collagenase D (Sigma) prepared in buffer (10 mM HEPES, pH 7.4, 150 mM NaCl, 5 mM KCl, 1 mM $MgCl_2$ and 1.8 mM $CaCl_2$) for 20 min. Then, the cell suspension was passed through a 100 µm cell strainer, harvested by centrifugation (500 x g for 7 min at 4ºC), washed twice with PBS and resuspended in RPMI medium (Gibco) supplemented with 10 mM HEPES, 1 mM sodium pyruvate, 1xRPMI 1640 vitamin mix, 10% (v/v) FBS, 50 U/mL penicillin and 50 µg/mL streptomycin, at 37 ºC under 5% CO_2 atmosphere. To test the antileishmanial activity of the different compounds against intramacrophagic amastigotes, the testing compounds were added to the explant seeded to confluence into 384-well black optical bottom plates (Thermo Scientific). The viability of amastigotes was calculated by recording their fluorescence

at 708 nm in an Odyssey (Li-Cor) infrared imaging system. Cell viability was used to determine the 50% effective concentration of the parasites in the amastigote form (EC_{50}).

6.2.3. Cytotoxicity and selectivity index (SI) determination

The cytotoxicity of the phosphorylated compounds was assessed on freshly isolated mouse splenocytes obtained from uninfected BALB/c mice, according to the previously described protocol. Viability of uninfected splenocytes was used to determine the 50% cytotoxic concentration (CC_{50}) using the Alamar Blue staining method, according to manufacturer's recommendations (Invitrogen). Selectivity index (SI) for each compound was calculated as the ratio between the CC_{50} value obtained for splenic cells and the EC_{50} value for amastigotes.

6.2.4. Purification of leishmanial and human TopIB

Expression and purification of leishmanial and human TopIB was performed according to a previously standardized protocol [72]. Briefly, both LTopIB and hTopIB were purified from the yeast strain EKY3 [MAT α ura3-52 his3Δ200 leu2Δ1 trp1Δ63 top1Δ: TRP1] which is deficient in TopIB activity and which had been transformed with the plasmids generated by joining the vector of bicistronic expression pESC-URA to both subunits of LTopIB or to the ORF of hTopIB. Yeasts were grown in yeast synthetic drop-out medium without uracil (Sigma) supplemented with 2% raffinose (w/v) to OD_{600}: 0.8-1 and induced for 10 h with 2% galactose (w/v). Cells were harvested, washed with cold TEEG buffer (50 mM Tris–HCl pH 7.4, 1 mM EDTA, 1 mM EGTA, 10% glycerol) and resuspended in 15 mL of 1 x TEEG buffer supplemented with 0.2 M KCl and a protease inhibitors cocktail (Thermo Scientific). Protein extract obtained after lysing yeast cells was loaded on a 5 mL Heparin Sepharose column (GEHealthcare). LTopIB enzyme was eluted at 4 ºC with a discontinuous gradient of KCl (0.2, 0.4, 0.6

771 M) in TEEG buffer and hTopIB was eluted with a discontinuous gradient of KCl (0.2,
772 0.4, 0.6, 0,8 M).

773 *6.2.5. TopIB relaxation activity assay*

774 The activity of both recombinant LTopIB and hTopIB enzymes was measured by the
775 relaxation of supercoiled plasmid DNA at 37º C. In a final volume of 20 µL, one unit of
776 purified LTopIB or hTopIB was incubated in the presence of 0.5 µg of supercoiled pSK
777 DNA, 10 mM Tris-HCl buffer pH 7.5, 5 mM $MgCl_2$, 0.1 mM EDTA, 15 µg/mL bovine
778 serum albumin and 180 mM KCl at different time points and stopped by the addition of
779 4 µL loading buffer (5% sarkosyl, 0,12% bromophenol blue, 25% glycerol). The DNA
780 topoisomers were resolved in 1% agarose gels by electrophoresis in 0.1 M Tris borate
781 EDTA buffer (pH 8.0) at 2 V/cm for 16 h and visualized with UV illumination after
782 ethidium bromide (0.5 µg/mL) staining. One unit of purified LTopIB or hTopIB enzyme
783 was incubated with different concentrations of each compound for 15 min at 37 ºC.

784 *6.3. Computational methodology*

785 *6.3.1. Molecular modeling*

786 All calculations included in this paper were carried out with Gaussian 16 program [73]
787 within the density functional theory (DFT) framework [63] using the B3LYP [64],
788 along with the standard 6-31G** basis set. All minima were fully characterized by
789 harmonic frequency analysis [74]. The solvent effect in DFT calculations was evaluated
790 by means of the Polarizable Continuum Model (PCM) [75] using water as solvent. The
791 pKa values were studied to determine the dominant species (ionization states) at
792 physiological pH (pH = 7.4) using Epik [76] and these were the species used in each
793 case. After a conformational search with MacroModel [77] the most stable
794 conformations were chosen and optimized at the B3LYP/6-31G** + ΔZPVE level of

theory and also were computed at the B3LYP(PCM)/6-31G** + ZPVE level using water as solvent. Among them, the most stable of each compound was chosen to calculate the molecular DFT-based parameters, molecular electrostatic potential energetics and docking studies. The obtained results for the molecular electrostatic potential surfaces were generated using GaussView Rev 5.0.9 [78].

6.3.2. Docking studies

First, we proceeded with the choice of the most suitable TopIB/DNA complex for the docking in the Protein Data Bank (PDB). The X-ray structure code 1T8I [65] (3.00 Å resolution) was chosen, a TopIB of human origin covalently bounded to DNA and containing the anti-cancer agent CPT as a ligand. Maestro [66] graphic interface was used, and the Glide 6.9 application [67] in XP mode (extra-precision) [68] was chosen for the docking. The grid was set up in a box of 20 x 20 x 20 Å, centered in the geometric center of CPT. The DNA-binding region in the active site was selected as the target for the screening. The TopIB/DNA complex was prepared by reconstructing the phosphoester bond to nucleobase C12 in the 1T8I structure, and the 5'-SH of nucleobase G11 of the cleaved strand was converted to a 5'-OH by changing the sulfur atom by an oxygen. The hydrogen atoms were added. The binding orders and the protonation states of waste and DNA were corrected. The complex was optimized and minimized using the Protein Preparation Wizard panel of Schrödinger Suites 2015.1 [79]. Likewise, the structures of the different ligands to be interacted with protein and the ligand initially present in the complex, CPT, were prepared as previously indicated and used for the different docking processes.

6.3.3. Predictive druggability

The predictive druggability of the phosphorus substituted quinoline derivatives were assessed using the physicochemical properties of lipophilic, electronic and structural

profiles in order to support the understanding of their antileishmanial–mechanism of action and the potential toxicity effects.

The compounds were also studied by applying the Rule of Five Lipinski, through the use of online free web cheminformatics software SwissAdme, where the following values were obtained: number of rotatable bonds (nRotB), molecular weight, empirical molecular structure and number of hydrogen acceptor groups (HBA) and hydrogen bond donors (HBD).

Acknowledgements

Financial support from the *Ministerio de Economía y Competitividad* (MINECO, AEI, FEDER, UE) [MINECO: AGL2016-79813-C2-1R, SAF2017-83575-R and CTQ2015-67871-R], *Gobierno Vasco* (GV, IT 992-16) and the *Junta de Castilla y León* cofinanced by FEDER, UE [LE020P17] is gratefully acknowledged. Technical and human support provided by IZO-SGI, SGIker (UPV/EHU, MICINN, GV/EJ, ERDF and ESF) is gratefully acknowledged.

Corresponding Author

*Phone: +34 945 013103; fax: +34 945 013049; e-mail: francisco.palacios@ehu.eus

References

[1] WHO/Department of Control of Neglected Tropical Diseases, Global leishmaniasis update, 2006-2015: a turning point in leishmaniasis surveillance, Weekly Epidemiological Record 38 (2017) 557-572.
[2] D. Pace, Leishmaniasis, J. Infect. 69 (2014) S10-S18.
[3] F. Frézard, C. Demicheli, R.R. Ribeiro, Pentavalent antimonials: new perspectives for old drugs, Molecules 14 (2009) 2317-2336.
[4] K.A. Winship, Toxicity of antimony and its compounds, Adverse Drug React Acute Poisoning Rev. 6 (1987) 67-90.
[5] S. Sundar, D.K. More, M.K. Singh, V.P. Singh, S. Sharma, A. Makharia, P.C. Kumar, H.W. Murray, Failure of pentavalent antimony in visceral leishmaniasis in India: report from the center of the Indian epidemic, Clin. Infect. Dis. 31 (2000) 1104–1107.
[6] M. Perry, S. Wyllie, V. Prajapati, J. Menten, A. Raab, J. Feldmann, D. Chakraborti, S. Sundar, M. Boelaert, A. Picado, A. Fairlamb, Arsenic, antimony, and *Leishmania*: has arsenic contamination of drinking water in India led to treatment- resistant kala-azar? Lancet 385 (2015) S80.

[7] A. Ponte-Sucre, F. Gamarro, J. C. Dujardin, M. P. Barrett, R. López-Vélez, R. García-Hernández, A. W. Pountain, R. Mwenechanya, B. Papadopoulou, Drug resistance and treatment failure in leishmaniasis: A 21st century challenge, PLoS Negl. Trop. Dis. 11 (2017) e0006052.

[8] C. Rodrigo, P. Weeratunga, S.D. Fernando, S. Rajapakse, Amphotericin B for treatment of visceral leishmaniasis: systematic review and meta-analysis of prospective comparative clinical studies including dose-ranging studies, Clin. Microbiol. Infect. 24 (2018) 591-598.

[9] G.M. Jensen, The care and feeding of a commercial liposomal product: liposomal amphotericin B (AmBisome®), J. Liposome Res. 27 (2017) 173-179.

[10] T.P. Dorlo, M. Balasegaram, J.H, Beijnen, P.J. de Vries, Miltefosine: a review of its pharmacology and therapeutic efficacy in the treatment of leishmaniasis, J. Antimicrob. Chemother. 67 (2012) 2576-2597.

[11] H. Sindermann, J. Engel, Development of miltefosine as an oral treatment for leishmaniasis, Trans R. Soc. Trop. Med. Hyg. 100 (2006) S17-20.

[12] F. Alves, G. Bilbe, S. Blesson, V. Goyal, S. Monnerat, C. Mowbray, G. Muthoni Ouattara, B. Pécoul, S. Rijal, J. Rode, A. Solomos, N. Strub-Wourgaft, M. Wasunna, S. Wells, E. E. Zijlstra, B. Arana, J. Alvar, Recent development of visceral leishmaniasis treatments: successes, pitfalls, and perspectives, Clin. Microbiol. Rev. 31 (2018) e00048-18.

[13] J. J. Champoux, DNA topoisomerases: structure, function, and mechanism, Annu. Rev. Biochem. 70 (2001) 369-413.

[14] L. Stewart, M.R. Redinbo, X. Qiu, W.G. Hol, J.J. Champoux, A model for the mechanism of human topoisomerase I, Science 279 (1998) 1534-1541.

[15] B.L. Staker, K. Hjerrild, M.D. Feese, C.A. Behnke, A.B. Burgin Jr, L. Stewart, The mechanism of topoisomerase I poisoning by a camptothecin analog, Proc. Natl. Acad. Sci. U. S. A. 99 (2002) 15387-15392.

[16] D.A. Koster, V. Croquette, C. Dekker, S. Shuman, N.H. Dekker, Friction and torque govern the relaxation of DNA supercoils by eukaryotic topoisomerase IB, Nature. 434 (2005) 671-674.

[17] Y. Pommier, Camptothecins and topoisomerase I: a foot in the door. Targeting the genome beyond topoisomerase I with camptothecins and novel anticancer drugs: importance of DNA replication, repair and cell cycle checkpoints, Curr. Med. Chem. Anticancer Agents. 4 (2004) 429-434.

[18] C. Bailly, Topoisomerase I poisons and suppressors as anticancer drugs, Curr. Med. Chem. 7 (2000) 39-58.

[19] Y.Q. Liu, W.Q. Li, S.L. Morris-Natschke, K. Qian, L. Yang, G.X. Zhu, X.B. Wu, A.L. Chen, S.Y. Zhang, X. Nan, K.H. Lee, Perspectives on biologically active camptothecin derivatives, Med. Res. Rev. 35 (2015) 753-789.

[20] W. Wei, S.J. Shi, J. Liu, X. Sun, K. Ren, D. Zhao, X.N. Zhang, Z.R. Zhang, T. Gong, Lipid nanoparticles loaded with 10-hydroxycamptothecin-phospholipid complex developed for the treatment of hepatoma in clinical application, J. Drug Target 18 (2010) 557–566.

[21] Y. Pommier, Drugging topoisomerases: lessons and challenges, ACS Chem. Biol. 8 (2013) 82-95.

[22] R.M. Reguera, C.M. Redondo, R. Gutiérrez de Prado, Y. Pérez-Pertejo, R. Balaña-Fouce. DNA topoisomerase I from parasitic protozoa: a potential target for chemotherapy. Biochim. Biophys. Acta. 1759 (2006), 117-131.

[23] R. Balaña-Fouce, R. Alvarez-Velilla, C. Fernández-Prada, C. García-Estrada, R.M. Reguera, Trypanosomatids topoisomerase re-visited. New structural findings and role in drug discovery, Int. J. Parasitol. Drugs Drug Resist. 4 (2014) 326-337.

[24] C.F. Prada, R. Alvarez-Velilla, R. Balaña-Fouce, C. Prieto, E. Calvo-Álvarez, J.M. Escudero-Martínez, J.M. Requena, C. Ordóñez, A. Desideri, Y. Pérez-Pertejo, R.M. Reguera, Gimatecan and other camptothecin derivatives poison *Leishmania* DNA-topoisomerase IB leading to a strong leishmanicidal effect, Biochem. Pharmacol. 85 (2013) 1433-1440.

[25] R. Balaña-Fouce, C.F. Prada, J.M. Requena, M. Cushman, Y. Pommier, R. Álvarez-Velilla, J.M. Escudero-Martínez, E. Calvo-Álvarez, Y. Pérez-Pertejo, R.M. Reguera, Indotecan (LMP400) and AM13-55: two novel indenoisoquinolines show potential for treating visceral leishmaniasis, Antimicrob. Agents Chemother. 56 (2012) 5264-5270.

[26] N.M. Carballeira, M. Cartagena, D. Sanabria, D. Tasdemir, C.F. Prada, R.M. Reguera, R. Balaña-Fouce, 2-Alkynoic fatty acids inhibit topoisomerase IB from *Leishmania donovani*, Bioorg. Med. Chem. Lett. 22 (2012) 6185-6189.

[27] (a) C. Viegas-Junior, A. Danuello, V. da Silva Bolzani, E. J. Barreiro, C. A. M. Fraga, Molecular hybridization: a useful tool in the design of new drug prototypes, Curr. Med. Chem. 14 (2007) 1829–1852;

(b) B. Meunier, Hybrid molecules with a dual mode of action: dream or reality**?** Acc. Chem. Res. 41 (2007) 69–77.

[28] G. Berube, An overview of molecular hybrids in drug discovery, Expert Opin. Drug Discov. 11 (2016) 281–305.
[29] S. M. Shaveta, S. Palvinder, Hybrid molecules: the privileged scaffolds for various pharmaceuticals, Eur. J. Med. Chem. 124 (2016) 500–536.
[30] (a) B.Nammalwar, R. A. Bunce, Recent syntheses of 1, 2,3,4-tetrahydroquinolines, 2,3-dihydro-4(1H)-quinolinones and 4(1H)-quinolinones using domino reactions, Molecules 19 (2014) 204–232;
(b) V. Sridharan, P. A. Suryavanshi, J. C. Menendez, Advances in the chemistry of tetrahydroquinolines, Chem. Rev. 111 (2011) 7157–7259.
[31] (a) S. Narwal, S. V. Kumar, K. Prabhakar, Synthesis and therapeutic potential of quinoline derivatives. Res. Chem. Int.,43 (2017) 2765–2798;
(b) P.-Y. Chung, Z.-X. Bian, H.-Y. Pun, D. Chan, A. S.-C. Chan, C.-H. Chui, J. C.-O. K.-H. Tang, Lam, Recent advances in research of natural and synthetic bioactive quinolines, Future Med. Chem. 7 (2015) 947–967.
[32] For reviews see: (a) A. Mucha, P. Kafarski, L. Berlicki, Remarkable Potential of the aminophosphonate/phosphinate structural motif in Medicinal Chemistry, J. Med. Chem. 54 (2011) 5955–5980;
(b) R. Engel in Handbook of Organophosphorus Chemistry M. Dekker Inc., New York, 1992;
(c) P. Kafarski, B. Lejezak, Biological activity of aminophosphonic acids, Phosphorus Sulfur 63 (1991) 193–215.
[33] F. Palacios, C. Alonso, J. M. de los Santos, Synthesis of β-aminophosphonates and -phosphinates. Chem. Rev. 105 (2005) 899–931.
[34] (a) D. Virieux, J. N. Volle, N. Bakalara, J. L. Pirat, Synthesis and biological applications of phosphinates and derivatives. Top. Curr. Chem. 360 (2015) 39–114;
(b) D. Virieux, N. Sevrain, T. Ayad, J. L. Pirat, Helical phosphorus derivatives, Adv. Heterocycl. Chem. 116 (2015) 37–83.
[35] For reviews see: (a) K. Van der Jeught, C. V. Stevens, Direct phosphonylation of aromatic azaheterocycles, Chem. Rev. 109 (2009) 2672–2702;
(b) K. Moneen, I. Laureyn, C. V. Stevens, Synthetic methods for azaheterocyclic phosphonates and their biological activity, Chem. Rev. 104 (2004) 6177–6215.
[36] A. De Blieck, K. G. R. Masschelein, F. Dhaene, E. Rozycka-Sokolowska, B. Marciniak, J. Drabowicz, C. V. Stevens, One-pot tandem 1,4–1,2-addition of phosphites to quinolines, Chem. Comm. 46 (2010) 258–260.
[37] A. Bykowska, R. Starosta, J. Jezierska, M. Jeżowska-Bojczuk, Coordination versatility of phosphine derivatives of fluoroquinolones. New CuI and CuII complexes and their interactions with DNA, RSC Adv. 5 (2015) 80804–80815.
[38] A. Emadi, R. J. Jones, R. A. Brodsky, Cyclophosphamide and cancer: golden anniversary, Nat Rev Clin Oncol. 6 (2009) 638–647.
[39] A. Markham, Brigatinib: first global approval, Drugs 77 (2017) 1131–1135.
[40] W.S. Huang, S. Liu, D. Zou, M. Thomas, Y. Wang, T. Zhou, J. Romero, A. Kohlmann, F. Li, J. Qi, L. Cai, T.A. Dwight, Y. Xu, R. Xu, R. Dodd, A. Toms, L. Parillon, X. Lu, R. Anjum, S. Zhang, F. Wang, J. Keats, S.D. Wardwell, Y. Ning, Q. Xu, L.E. Moran, Q.K. Mohemmad, H.G. Jang, T. Clackson, N.I. Narasimhan, V.M. Rivera, X. Zhu, D. Dalgarno, W.C. Shakespeare, Discovery of Brigatinib (AP26113), a phosphine oxide-containing, potent, orally active inhibitor of anaplastic lymphoma kinase, J. Med. Chem. 59 (2016) 4948–4964.
[41] J. R. Chekan, D. P. Cogan, S. K. Nair, Molecular basis for resistance against phosphonate antibiotics and herbicides, Med. Chem. Commun. 7 (2016) 28–36.
[42] E. Vitaku, D. T. Smith, J. T. Njardarson, Analysis of the structural diversity, substitution patterns, and frequency of nitrogen heterocycles among U.S. FDA approved pharmaceuticals, J. Med. Chem. 57 (2014) 10257−10274.
[43] (a) C. Cabrele, O.Reiser, The modern face of synthetic heterocyclic chemistry, J. Org. Chem. 81 (2016) 10109–10125;
(b) S. L. Schreiber, Target-oriented and diversity-oriented organic synthesis in drug discovery, Science 287 (2000) 1964–1969.
[44] K. M. Shea, Name reactions for carbocyclic ring formations, J. J. Li (Ed); Wiley, Hoboken: NJ, 2010, pp. 275–308.
[45] (a) D. H. Ess, G.O. Jones, K.N. Houk, Conceptual, qualitative, and quantitative theories of 1,3-dipolar and Diels–Alder cycloadditions used in synthesis, Adv. Synth. Catal. 348 (2006) 2337–2361;
(b) K.C. Nicolaou, S.A. Snyder, T. Montagnon, G. Vassilikogiannakis, The Diels–Alder reaction in total synthesis, Angew. Chem., Int. Ed. 41 (2002) 1668–1698.

[46] (a) S. Seghers, L. Protasova, S. Mullens, J.W. Thybaut, C.V. Stevens, Improving the efficiency of the Diels–Alder process by using flow chemistry and zeolite catalysis, Green Chem. 19 (2017) 237–248;
(b) J.-A. Funel, S. Abele, Industrial applications of the Diels–Alder reaction, Angew. Chem., Int. Ed. 52 (2013) 3822–3863.
[47] For reviews see: (a) J. S. Bello, J. Jones, F. M. da Silva, The Povarov reaction as a versatile strategy for the preparation of 1, 2,3,4-tetrahydroquinoline derivatives: an overview, Curr. Org. Synth. 13 (2016) 157–175;
(b) G. Masson, C. Lalli, M. Benohoud, G. Dagousset, Catalytic enantioselective [4 + 2]-cycloaddition: a strategy to access aza-hexacycles, Chem. Soc. Rev. 42 (2013) 902–923;
(c) E. Vicente-Garcia, R. Ramon, R. Lavilla, New heterocyclic inputs for the Povarov multicomponent reaction, Synthesis (2011) 2237–2246.
[48] For recent contributions see: (a) T. Selvi, S. Velmathi, Indium(III) triflate-catalyzed reactions of aza-Michael adducts of chalcones with aromatic amines: retro-Michael addition versus quinoline formation, J. Org. Chem. 83 (2018) 4087−4091;
(b) P. A. S. Abranches, W. F. de Paiva, A. de Fatima, F. T. Martins, S. A. Fernandes, Calix[n]arene-Catalyzed Three-Component Povarov Reaction: Microwave-Assisted Synthesis of Julolidines and Mechanistic Insights, J. Org. Chem. 83 (2018) 1761−1771;
(c) N. Goli, S. Kallepu, P. S. Mainkar, J. K. Lakshmi, R. Chegondi, S. Chandrasekhar, Synthetic Strategy toward the Pentacyclic Core of Melodinus Alkaloids, J. Org. Chem. 83 (2018) 2244−2249.
[49] (a) W. Dong, Y. Yuan, B. Hu, X Gao, H. Gao, X. Xie, Z. Zhang, Combining visible-light-photoredox and Lewis acid catalysis for the synthesis of indolizino[1,2-b]quinolin-9(11H)-ones and irinotecan precursor, Org. Lett. 20 (2018) 80–83;
(b) A. I. Almansour, N. Arumugam, K. R. Suresh Kumar, S. M. Mahalingam, S. Sau, G. Bianchini, J. C. Menendez, M. Altaf, H. A. Ghabbour, Design, synthesis and antiproliferative activity of decarbonyl luotonin analogues, Eur. J. Med. Chem. 138 (2017) 932–941.
[50] (a) C. Alonso, M. Fuertes, M. González, G. Rubiales, C. Tesauro, B. R. Knudsen, F. Palacios, Synthesis and biological evaluation of indeno[1,5]naphthyridines as topoisomerase I (TopI) inhibitors with antiproliferative activity, Eur. J. Med. Chem. 115 (2016) 179–190;
(b) F. Palacios, C. Alonso, M. Fuertes, J. M. Ezpeleta, G. Rubiales, Glyoxalate-derived aldimines in cycloaddition reactions with olefins, Eur. J. Org. Chem. (2011) 4318–4326;
(c) C. Alonso, M. González, G. Rubiales, F. Palacios, Study of the hetero-[4+2]-cycloaddition reaction of aldimines and alkynes. Synthesis of 1,5-naphthyridine and isoindolone derivatives, J. Org. Chem. 82 (2017) 6379−6387.
[51] O. Ghashghaei, C. Masdeu, C. Alonso, F. Palacios, R. Lavilla, Recent advances of the Povarov reaction in medicinal chemistry, Drug Discov. Today 23 (2018), 0000.
[52] C. Alonso, M. Fuertes, E. Martin-Encinas, A. Selas, G. Rubiales, C. Tesauro, B. R. Knudsen, F. Palacios, Novel topoisomerase I inhibitors. Syntheses and biological evaluation of phosphorus substituted quinoline derivates with antiproliferative activity, Eur. J. Med. Chem. 149 (2018) 225–237.
[53] (a) A. Tejería, Y. Pérez-Pertejo, R. M. Reguera, R. Balaña-Fouce, C. Alonso, M. González, G. Rubiales, F. Palacios, Substituted 1,5-naphthyridine derivatives as novel antileishmanial agents. Synthesis and biological evaluation, Eur. J. Med. Chem. 152 (2018) 137–147;
(b) A. Tejería, Y. Pérez-Pertejo, R. M. Reguera, R. Balaña-Fouce, C. Alonso, M. Fuertes, M. González, G. Rubiales, F. Palacios, Antileishmanial effect of new indeno-1,5-naphthyridines, selective inhibitors of Leishmania infantum type IB DNA topoisomerase, Eur. J. Med. Chem. 124 (2016) 740–749.
[54] C. Alonso, E. Martín-Encinas, G. Rubiales, F. Palacios Reliable synthesis of phosphino- and phosphine sulfide-1,2,3,4-tetrahydroquinolines and phosphine sulfide quinolines, Eur. J. Org. Chem. (2017) 2916–2924.
[55] Fluorine substituents are important fragments of commercial drugs. C. Alonso, E. Martinez de Marigorta, G. Rubiales, F. Palacios, Carbon trifluoromethylation reactions of hydrocarbon derivatives and heteroarenes, Chem. Rev. 115 (2015) 1847–1935.
[56] E. Calvo-Álvarez, K. Stamatakis, C. Punzón, R. Álvarez-Velilla, A. Tejería, J.M. Escudero-Martínez, Y. Pérez-Pertejo, M. Fresno, R. Balaña-Fouce, R.M. Reguera, Infrared fluorescent imaging as a potent tool for in vitro, ex vivo and in vivo models of visceral leishmaniasis, PLoS Negl. Trop. Dis. 9 (2015) e0003666.
[57] Y. Osorio, B.L. Travi, A.R. Renslo, A.G. Peniche, P.C. Melby, Identification of small molecule lead compounds for visceral leishmaniasis using a novel ex vivo splenic explant model system. PLoS Negl. Trop. Dis. 5 (2011) e962.

[58] R. Diaz-González, Y. Pérez-Pertejo, Y. Pommier, R. Balaña-Fouce, R.M. Reguera, Mutational study of the "catalytic tetrad" of DNA topoisomerase IB from the hemoflagellate Leishmania donovani: Role of Asp-353 and Asn-221 in camptothecin resistance, Biochem. Pharmacol. 76 (2008) 608-619.
[59] S. J. Froelich-Ammon, N. Osheroff, Topoisomerase poisons: harnessing the dark side of enzyme mechanism, J. Biol. Chem. 270 (1995) 21429-21432.
[60] A. Coletta, A. Desideri, Role of the protein in the DNA sequence specificity of the cleavage site stabilized by the camptothecin topoisomerase IB inhibitor: a metadynamics study, Nucleic Acids Res. 41 (2013) 9977-9986.
[61] Since compound **6a** was previously reported as hTopIB, we tried to assay it at shorter time (below 2 min) and we found weak but appreciable inhibition at both 1 and 2 min (results not found)
[62] M. A. Bhat, S. H. Lone, M. A. Mir, S. A. Majid, H. M. Bhat, R. J. Butcher, S. K. Srivastava, Synthesis of t-butyl 2-(4-hydroxy-3-methoxybenzylidene)hydrazine carboxylate: Experimental and theoretical investigations of its properties, J. Mol. Struct. 1164 (2018) 516–524 and references therein cited.
[63] (a) R. G. Parr, W. Yang, Density-Functional Theory of Atoms and Molecules; Oxford University Press: Oxford, 1989. (b) T. Ziegler, Approximate density functional theory as a practical tool in molecular energetics and dynamics, Chem. Rev. 91 (1991) 651–667.
[64] (a) W. Kohn, A. D. Becke, R. G. Parr, Density Functional Theory of Electronic Structure, J. Phys. Chem. 100 (1996) 12974–12980. (b) A. D. Becke, Density-functional thermochemistry. III. The role of exact exchange, J. Chem. Phys. 98, (1993) 5648-5652. (c) A. D. Becke, Density-functional exchange-energy approximation with correct asymptotic behaviour, Phys. Rev. A 38, (1998) 3098–3100.
[65] B. L. Staker, M. D. Feese, M. Cushman, Y. Pommier, D. Zembower, L. Stewart, A. B. Burgin, Structures of three classes of anticancer agents bound to the human topoisomerase I-DNA covalent complex, J. Med.Chem. 48 (2005) 2336-2345.
[66] Schrödinger Release 2015-1: Maestro, version 10.1, Schrödinger, L.L.C.: New York, 2015.
[67] Schrödinger Release 2015-1: Glide, version 6.9, Schrödinger, L.L.C.: New York, 2015
[68] (a) R. A. Friesner, R. B. Murphy, M. P. Repasky, L. L. Frye, J. R. Greenwood, T. A. Halgren, P. C. Sanschagrin, D. T. Mainz, Extra precision glide: docking and scoring incorporating a model of hydrophobic enclosure for protein-ligand complexes, J. Med. Chem. 49 (2006) 6177-6196;
(b) R. A. Friesner, J. L. Banks, R. B. Murphy, T. A. Halgren, J. J. Klicic, D. T. Mainz, M. P. Repasky, E. H. Knoll, M. Shelley, J. K. Perry, D. E. Shaw, P. Francis, P. S. Shenkin, Glide: a new approach for rapid, accurate docking and scoring. 1. Method and assessment of docking accuracy, J. Med. Chem. 47 (2004) 1739–1749.
[69] (a) N. M. Baker, R. Rajan, A. Mondragón, Structural studies of type I topoisomerases, Nucleic Acids Res. 37 (2009) 693-701;
(b) C. Marchand, S. Antony, K. W. Kohn, M. Cushman, A. Ioanoviciu, B. L. Staker, A. B. Burgin, L. Stewart, Y. Pommier, A novel norindeniosoquinoline structure reveals a common interfacial inhibitor paradigm for ternary trapping of the topoisomerase I-DNA covalent complex, Mol. Cancer Ther. 5 (2006) 287-295;
(c) D. A. Koster, K. Paile, E. S. M. Bot, M. A. Bjornsti, N. H. Dekker, Antitumour drugs impede DNA uncoiling by topoisomerase I, Nature 448 (2007) 213-217;
(d) A. Lauria, M. Ippolito, A. M. Almerico, Molecular docking approach on the Topoisomerase I inhibitors series included in the NCI anti-cancer agents mechanism database, J. Mol. Model. 13 (2007) 393-400.
[70] G.Chillemi, L. Fiorami, P. Benedetti, A. Desideri, Protein concerted motions in the DNA–human topoisomerase I complex, Nucleic. Acids Res. 31 (2003) 1525-1535.
[71] Y. Pommier, C. Marchand, Interfacial inhibitors: targeting macromolecular complexes, Nature Rev. 11 (2012) 25–36.
[72] H. Villa, A.R. Otero Marcos, R.M. Reguera, R. Balaña-Fouce, C. García-Estrada, Y. Pérez-Pertejo, B.L. Tekwani, P.J. Myler, K.D. Stuart, M.A. Bjornsti, D. Ordóñez, A novel active DNA topoisomerase I in *Leishmania donovani*, J. Biol. Chem. 278 (2003) 3521-3526.
[73] Gaussian 16, Revision A.03, M. J. Frisch, G. W. Trucks, H. B. Schlegel, G. E. Scuseria, M. A. Robb, J. R. Cheeseman, G. Scalmani, V. Barone, G. A. Petersson, H. Nakatsuji, X. Li, M. Caricato, A. V. Marenich, J. Bloino, B. G. Janesko, R. Gomperts, B. Mennucci, H. P. Hratchian, J. V. Ortiz, A. F. Izmaylov, J. L. Sonnenberg, D. Williams-Young, F. Ding, F. Lipparini, F. Egidi, J. Goings, B. Peng, A. Petrone, T. Henderson, D. Ranasinghe, V. G. Zakrzewski, J. Gao, N. Rega, G. Zheng, W. Liang, M. Hada, M. Ehara, K. Toyota, R. Fukuda, J. Hasegawa, M. Ishida, T. Nakajima, Y. Honda, O. Kitao, H. Nakai, T. Vreven, K. Throssell, J. A. Montgomery, Jr., J. E. Peralta, F. Ogliaro, M. J. Bearpark, J. J. Heyd, E. N. Brothers, K. N. Kudin, V. N. Staroverov, T. A. Keith, R. Kobayashi, J. Normand, K.

Raghavachari, A. P. Rendell, J. C. Burant, S. S. Iyengar, J. Tomasi, M. Cossi, J. M. Millam, M. Klene, C. Adamo, R. Cammi, J. W. Ochterski, R. L. Martin, K. Morokuma, O. Farkas, J. B. Foresman, and D. J. Fox, Gaussian, Inc., Wallingford CT, 2016.
[74] J. W. Mciver Jr, A. J. Komornicki, Structure of transition states in organic reactions. General theory and an application to the cyclobutene-butadiene isomerization using a semiempirical molecular orbital method, J. Am. Chem. Soc. 94, (1972) 2625–2633.
[75] (a) S. Miertus, E. Scrocco, J. J. Tomasi, Electrostatic interaction of a solute with a continuum. A direct utilizaion of AB initio molecular potentials for the prevision of solvent effects, Chem. Phys. 55, (1981) 117–129. (b) B. Mennucci, J. J. Tomasi, Continuum solvation models: A new approach to the problem of solute's charge distribution and cavity boundaries, Chem. Phys. 106, (1997) 5151–5158. (c) R. Cammi, B. Mennucci, J. J. Tomasi, Fast Evaluation of Geometries and Properties of Excited Molecules in Solution: A Tamm-Dancoff Model with Application to 4-Dimethylaminobenzonitrile, Phys. Chem. A 104 (2000) 5631–5637. (d) For an entry to the Polarized Continuum Model (PCM, solvent effects), see: J. Tomasi, B. Mennucci, R. Cammi, Quantum Mechanical Continuum Solvation Models, Chem. Rev. 105 (2005) 2999–3094.
[76] Schrödinger Release 2015-1: Epik, version 3.1, Schrödinger, L.L.C.: New York, 2015.
[77] Macro Model, Schrödinger, LLC, New York, NY 2018.
[78] GaussView, Rev 5.0.9: R. Dennington, Todd A. Keith, and John M. Millam, Semichem Inc., Shawnee Mission, KS, 2016.
[79] Schrödinger Release 2015-1: Protein Preparation Wizard, Epik 3.1, Schrödinger, L.L.C.: New York, 2015.

List of Captions

Figure 1. Structure of miltefosine (left), camptothecin (middle) and newly phosphorated tetrahydroquinolines and quinolines (right).

Figure 2. MEP surfaces mapped from total electron density for compounds **4** to **8**. Electrostatic potentials are displayed on a 0.002 a.u. isodensity surface. The limits of electrostatic potentials for each molecule are under surfaces. Potential increases in the following order: red (most negative)/orange/yellow/green/blue (most positive).

Figure 3. The 2D interaction of compounds **4a** (A), **4b** (B), **4c**(C), **7a** (D) and **8c** (E) in the binding site of hTop1B. (For interpretation of the references to colour in this figure legend, the reader is referred to the web version of this article).

Figure.4. The potential binding modes of compounds **4a** (A, in blue), **4b** (B in yellow), **4c** (C in lime green), **7a** (D in purple) and **8c** (E in red) with hTop1B (PDB code: 1T8I). The key residues of the protein were colored in dark green, and DNA bases by the atom type. The hydrogen bond for **8c** (in E) was shown with yellow dashed line. (For interpretation of the references to colour in this figure legend, the reader is referred to the web version of this article).

Scheme 1. Syntheses of 1,2,3,4-tetrahydroquinolinyl-phosphines **4**, -phosphine sulfides **5**, -phosphine oxides **6**, quinolinyl-phosphine sulfides **7** and -phosphine oxides **8** [a]

Chart 1. Structures of 1,2,3,4-tetrahydroquinolinylphosphines **4**, -phosphine sulfides **5**, and -phosphine oxides **6** obtained by multicomponent Povarov reaction.

Chart 2. Structures of quinolinyl-phosphine sulfides **7** and -phosphine oxides **8** obtained by dehydrogenation.

1134 **Table 1.** Bioactivity of phosphorylated compounds on both forms of Leishmania
1135 parasites.

1136 **Table 2.** Inhibition of relaxation activity of LTopIB and hTopIB by phosphorus
1137 containing quinoline derivatives.

1138 **Table 3.** Calculated energies and molecular proprieties computed at B3LYP/6-31G**
1139 basis set level of theory for compounds **4** to **8**.

1140 **Table 4**. gscore and gemodel values for best hTopIB inhibitors.